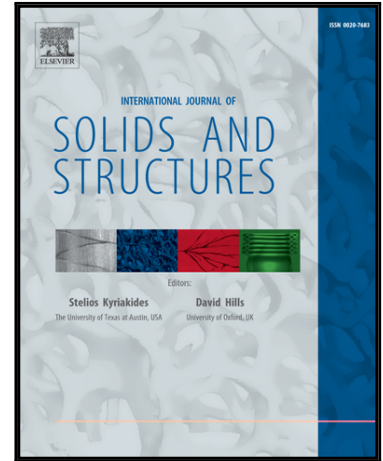


Accepted Manuscript

Buckling analysis of variable angle tow composite plates with a through-the-width or an embedded rectangular delamination

Xiaodong Chen , Zhangming Wu , Guojun Nie , Paul Weaver

PII: S0020-7683(18)30011-8
DOI: [10.1016/j.ijsolstr.2018.01.010](https://doi.org/10.1016/j.ijsolstr.2018.01.010)
Reference: SAS 9859



To appear in: *International Journal of Solids and Structures*

Received date: 12 July 2017
Revised date: 9 November 2017
Accepted date: 9 January 2018

Please cite this article as: Xiaodong Chen , Zhangming Wu , Guojun Nie , Paul Weaver , Buckling analysis of variable angle tow composite plates with a through-the-width or an embedded rectangular delamination, *International Journal of Solids and Structures* (2018), doi: [10.1016/j.ijsolstr.2018.01.010](https://doi.org/10.1016/j.ijsolstr.2018.01.010)

This is a PDF file of an unedited manuscript that has been accepted for publication. As a service to our customers we are providing this early version of the manuscript. The manuscript will undergo copyediting, typesetting, and review of the resulting proof before it is published in its final form. Please note that during the production process errors may be discovered which could affect the content, and all legal disclaimers that apply to the journal pertain.

Buckling analysis of variable angle tow composite plates with a through-the-width or an embedded rectangular delamination

Xiaodong Chen ^a; Zhangming Wu ^{b, a, *}; Guojun Nie ^a; Paul Weaver ^{c, d}

^a School of Aerospace Engineering and Applied Mechanics, Tongji University, 200092, China

^b Cardiff School of Engineering, Cardiff University, The Parade, Cardiff CF24 3AA, UK

^c ACCIS, University of Bristol, University Walk, Bristol BS8 1TR, UK

^d Bernal Institute, University of Limerick, Ireland

Corresponding Author: Zhangming Wu * E-mail: wuz12@cardiff.ac.uk; z.wu@tongji.edu.cn

Abstract: Variable angle tow (VAT) composite laminates, in which fibre orientation varies spatially in-plane in a continuous fashion yet is piecewise constant through-thickness, have been made possible by advanced automated fibre placement technology. Such designs have shown considerable potential to improve the performance of lightweight composite structures. In the present study, an analytical model is developed to study the buckling behaviour of VAT composite plates with a through-the-width or an embedded rectangular delamination under compression loadings. The proposed model can accurately capture the global, local and mixed buckling response of delaminated VAT composite plates. Both free and constrained modes are assumed in the delamination buckling analysis. A constrained point approach is employed to analyze the buckling response when contact occurs between delaminated layers. The accuracy and reliability of this proposed delamination buckling model is validated by finite element analysis and with prior results. The influence of delamination size, position and varying fibre orientation angles on the buckling response of delaminated VAT composite plates is studied by numerical examples. It is shown that the buckling loads decrease with an increase of the delamination size. The VAT laminates with an off-midplane delamination may lead to the delamination opening up, which further reduces the buckling loads. Finally, the mechanism of taking advantages of VAT laminates to improve the buckling performance of delaminated composite plates is thoroughly investigated in a parametric study. This study also shows that the residual buckling resistance of the delaminated composite plates can be significantly improved through using the VAT design concept.

Keywords: variable angle tow; delamination; buckling; composites

1 Introduction

Many previous works [1-7] have shown that the buckling and postbuckling load-carrying capacity of composite structures can be significantly increased by using Variable Angle Tow (VAT) laminates. This enhanced performance is mainly attributed to the benign load

redistribution achieved by the variable stiffness properties of VAT laminates. However, composite laminates, due to their relatively weak interlaminar strength, are often prone to delamination (separation of adjoining plies), which is one of the most common failure mechanisms of composites. The presence of delamination may prematurely lead to the failure of composite laminates initiated by buckling, and therefore result in significant reduction in load-carrying capacity.

A considerable amount of research effort has been devoted to the study of structural behaviour of composite laminates with delaminations. Chai et al. [8] initially proposed a one-dimensional analytical model to assess the buckling strength of composite laminated beam-plates with a through-the-width delamination. Afterwards, Simitse et al. [9] employed the perturbation method to predict the buckling loads of composite beam-plates with a single delamination of various sizes and locations. The effects of delamination position and size on the buckling load of delaminated beam-plates were investigated in [9]. Kardomateas and Schmueser [10] extended the model proposed by Simitse et al. [9] to account for the transverse shear effect and investigated the buckling and postbuckling characteristics of beam-plates with a through-the-width delamination. Later, Kutlu and Chang [11] performed an analytical and experimental study on the compression behaviour, from initial loading to final collapse, of composite laminated beam-plates with multiple through-the-width delaminations. Lee et al. [12] developed a finite element model based on the layer-wise plate theory to solve the buckling problem of axially loaded composite laminated beam-plates with multiple delaminations. Chattopadhyay and Gu [13] developed a higher order plate theory to perform buckling analysis of composite beam-plates with through-the-width delamination. Shu [14] performed an exact buckling analysis of one-dimensional beam-plates with double delaminations based on the classical beam theory. Both free and constrained modes were identified in his delamination buckling analysis, which give the lower and upper bounds of residual buckling resistance, respectively. Bruno and Greco [15] investigated the delamination buckling and growth of beam-plates with a through-the-width delamination using asymptotic approach and energy release rate concept. In their work, global buckling of the whole plate occurs accompanied by a local instability of the delaminated sublaminates. Most of these studies employed one-dimensional analytical models to perform the buckling analysis of composite laminated beam-plates with a through-the-width delamination.

Two-dimensional modelling and analysis for composite laminates with embedded delaminations have also been presented by many researchers. Shivakumar and Whitcomb [16], Chai and Babcock [17] and Yin and Jane [18] investigated the compressive stability of an elliptically-shaped surface layer that had been debonded from a quasi-isotropic base laminate. In their works, the in-plane dimension of the debonded surface layer was assumed to be small compared to that of the parent substrate, but large compared to the layer thickness. Moreover,

Chai [19] studied the buckling and postbuckling response of the surface layer debonded from a parent laminate under uniform axial compression. The debonded surface layer was modelled as a unilaterally constrained plate to simulate the near-surface delamination problem and the contact problem between the two sublaminates at the delamination interface was considered. Shahwan and Waas [20] proposed another analytical study on the contact buckling of a debonded surface layer, in which they introduced a nonlinear elastic foundation that exhibits a deformation sign dependent force-displacement relationship to model the unilateral constraint problem. These studies on two-dimensional buckling analysis were mainly restricted to the near-surface composite layer debonded from a parent substrate. Under such circumstances, only local buckling could be captured in their delamination buckling analysis. However, a deep understanding on the mechanism of interaction between the sublaminates and the substrate during the delamination buckling is vitally important to the damage tolerance design of the whole composite plate with delaminations. Suemasu et al. [21-23] investigated the compressive buckling behavior of composite laminated plates with multiple embedded circular delaminations located at regular intervals along the thickness direction, both theoretically and experimentally. Kim and Kedward [24] presented an analytical model for the local buckling analysis of the delaminated sublaminates and global buckling analysis of composite laminated plates with an embedded delamination using Rayleigh-Ritz approximation technique. However, their analytical model does not capture the mixed buckling response of delaminated composite plates. Recently, Ovesy and co-workers [25, 26] investigated the buckling behaviour of composite laminated plates with an embedded rectangular delamination using the CPLT, FSDT and HSDT plate theories. However, all of the above research works on delamination buckling focused on constant stiffness laminated plates. So far, only a few researchers have attempted to study the delamination problems for variable stiffness composite structures. Butler et al. [27] applied the finite strip method to study the compression after impact (CAI) performance of delaminated VAT composite plates. Yazdani et al. [28] utilized XFEM (Extended Finite Element Method) to analyze the delamination propagation of VAT composite laminates. To the best of the authors' knowledge, no research has been reported in which an attempt has been made to investigate the buckling behaviour of VAT composite plates with delaminations. This work is the first study investigating the effects of rectangular delamination (type, size and position) on the residual buckling strength of VAT composite laminates.

In the present study, an analytical model with a generalized Rayleigh-Ritz approach is developed to study the characteristics of the buckling response of VAT composite plates with a through-the-width or an embedded rectangular delamination under axial compressive loading. The analytical model is derived from the potential energy expression based on classical laminated plate theory. The delamination buckling behaviour is modelled by a superposition of global and local displacement shape functions in which the kinematic continuity conditions

along the delamination edge are satisfied. Both free and constrained modes are assumed in the delamination buckling analysis. The potential contact problem is addressed using the constrained point approach. The prebuckling analysis is performed first to determine the highly non-uniform stress distribution of VAT plates that are subjected to displacement controlled loads. The buckling load and its corresponding mode shape under either a free or a constrained condition can be directly determined by the proposed analytical model. This model is capable of accurately simulating the global, mixed and local buckling behaviour for delaminated VAT composite plates. Moreover, the delamination buckling behaviour can also be accurately captured under situations where contact occurs.

The remainder of this work is organized as follows: in the next section, VAT composite plates with linear variation of fibre orientation angles are introduced. Section 3 presents the theoretical formulation in the modelling procedure of VAT composite plates with a single delamination, including the constitutive equation, the boundary conditions and the kinematic continuity conditions along the delamination edge. In section 4, the prebuckling and buckling problems of VAT composite plates with a through-the-width or an embedded rectangular delamination are solved using the Rayleigh-Ritz approach, based on the principle of minimum potential energy. The constrained point approach is employed to prevent the potential contact problem at the delamination interface. In section 5, numerical results obtained by the present model are compared with the FEM (Finite Element Method) simulation results and that given in previous works. In addition, the influence of delamination (type, size and position) and the potential contact problem on the buckling behaviour of delaminated VAT composite plates is investigated by numerical examples. The mechanism of exploiting variable stiffness properties to improve the residual buckling strength of composite plates with a rectangular delamination is also studied in detail. Finally, some conclusions are drawn in section 6.

2 VAT Laminates

The orientation of fibre angles of each ply of VAT composite plates are continuously varied with respect to the coordinates x and y , that also have the dual purpose of representing variable stiffness properties. As such, VAT composite plates provide extended design flexibility to potentially enhance structural performance. Generally, the fibre angle variation of a VAT plate is represented in a mathematical form using a small number of fibre angle parameters [7]. In this work, for simplicity, the VAT plate with a linear fibre angle variation is considered [29] and the angle variation along the x direction is given by

$$\theta(x) = \phi + \frac{2(T_1 - T_0)}{a}|x| + T_0 \quad (1)$$

where $\phi + T_0$ is the fibre orientation angle at the panel center $x=0$, $\phi + T_1$ is the fibre

orientation angle at the panel ends $x = \pm a/2$ and ϕ is the angle of rotation of the fibre path.

3 Theoretical formulation

3.1 Constitutive relation and strain-displacement relation

Consider a VAT composite plate of length a , width b and thickness h , with a single delamination, as shown in Fig. 1(a). The single delamination is located at the center of the plane of the plate, and the distance from the delamination interface to the top surface is h_1 . The VAT composite plate is divided into three portions by the existing delamination interface, namely, an undelaminated portion, denoted by 0, and two delaminated portions, denoted by 1 and 2, as shown in Fig. 1 (a). The constitutive equations for the L^{th} portion of the delaminated VAT composite plate are given in the following matrix form [30]

$$\begin{Bmatrix} \mathbf{N}^L \\ \mathbf{M}^L \end{Bmatrix} = \begin{bmatrix} \mathbf{A}^L & \mathbf{B}^L \\ \mathbf{B}^L & \mathbf{D}^L \end{bmatrix} \begin{Bmatrix} \boldsymbol{\varepsilon}^L \\ \boldsymbol{\kappa}^L \end{Bmatrix} \quad (L=0,1,2) \quad (2)$$

where $\mathbf{N}^L = \{N_{xx}^L \ N_{yy}^L \ N_{xy}^L\}^T$ and $\mathbf{M}^L = \{M_{xx}^L \ M_{yy}^L \ M_{xy}^L\}^T$ are the resultant force and bending moment vectors of the L^{th} portion, respectively. $\boldsymbol{\varepsilon}^L = \{\varepsilon_{xx}^L \ \varepsilon_{yy}^L \ \varepsilon_{xy}^L\}^T$ and $\boldsymbol{\kappa}^L = \{\kappa_{xx}^L \ \kappa_{yy}^L \ \kappa_{xy}^L\}^T$ are the mid-plane strain and curvature vectors of the L^{th} portion, respectively. \mathbf{A}^L , \mathbf{B}^L and \mathbf{D}^L are the in-plane, coupling and bending stiffness matrices of the L^{th} portion, respectively, and are expressed as [30]

$$A_{ij}^L = \sum_{k=1}^{K^L} Q_{ij}^k (z_{k+1} - z_k), B_{ij}^L = \frac{1}{2} \sum_{k=1}^{K^L} Q_{ij}^k (z_{k+1}^2 - z_k^2), D_{ij}^L = \frac{1}{3} \sum_{k=1}^{K^L} Q_{ij}^k (z_{k+1}^3 - z_k^3) \quad (3)$$

where $i, j = 1, 2, 6$ and K^L is the total number of plies of the L^{th} portion. z_k is the location of the k^{th} ply with respect to the mid-plane of each portion along the thickness direction. Q_{ij}^k is the reduced transformed stiffness terms of the k^{th} ply in each portion, which varies as a function of the coordinates x and y . For the case that each portion of delaminated VAT composite plate is symmetric with respect to the mid-plane of the corresponding portion, the coupling stiffness matrix \mathbf{B}^L in Eq. (2) vanishes. However, the delaminated VAT composite plate, if subjected to foreign object impact, may not be symmetric within each delaminated portion. Under such circumstances, the bending-extension coupling within each delaminated portion is taken into account using the method of reduced bending stiffness (RBS) [31], by which the stress resultants are not coupled to the plate curvatures and only related to the curvatures with a reduced stiffness matrix, $[\mathbf{D}^L] - [\mathbf{B}^L]^T [\mathbf{A}^L]^{-1} [\mathbf{B}^L]$.

Based on classical laminated plate theory, the strain-displacement relation of the L^{th} portion in the linear regime can be written as [30],

$$\varepsilon_{xx}^L = \frac{\partial u_L}{\partial x}, \varepsilon_{yy}^L = \frac{\partial v_L}{\partial y}, \varepsilon_{xy}^L = \frac{\partial u_L}{\partial y} + \frac{\partial v_L}{\partial x} \quad (L=0,1,2) \quad (4a)$$

$$\kappa_{xx}^L = -\frac{\partial^2 w_L}{\partial x^2}, \kappa_{yy}^L = -\frac{\partial^2 w_L}{\partial y^2}, \kappa_{xy}^L = -2\frac{\partial^2 w_L}{\partial x \partial y} \quad (L=0,1,2) \quad (4b)$$

where u_L and v_L are the in-plane displacements of the L^{th} portion and w_L the out-of-plane displacement of the L^{th} portion.

3.2 Boundary conditions and continuity conditions

Although this paper only studies VAT composite plates under compression loading, the proposed approach for solving the delamination buckling problem of VAT plates is general in terms of boundary conditions and loading cases. In this work, only the delaminated VAT beam-plate or plate loaded by uniform axial compression with transverse edges free to deform is taken into account. This is a mixed in-plane boundary condition, as shown in Fig. 1 (b) or (c), which can be expressed as

$$\bar{N}_{yy} = 0, \bar{N}_{yx} = 0 \quad \text{at } y = \pm b/2 \quad (5a)$$

$$u_0 = \mp \Delta / 2 \quad \text{at } x = \pm a/2 \quad (5b)$$

where the terms \bar{N}_{yy} and \bar{N}_{yx} are the boundary forces on the edges ($y = \pm b/2$). Δ is the prescribed uniform end-shortening loading. Two different types of the rectangular delamination are considered for VAT plates. The first one is a VAT plate with a through-the-width delamination, as shown in Fig. 1 (b). For this case, the boundary conditions are simply supported or clamped at edges ($x = \pm a/2$) and are free on the edges ($y = \pm b/2$), and can be expressed as,

$$w_0 = 0 \quad \text{at } x = \pm a/2 \quad (\text{simply supported}) \quad (6a)$$

$$w_0 = 0, \frac{\partial w_0}{\partial x} = 0 \quad \text{at } x = \pm a/2 \quad (\text{clamped}) \quad (6b)$$

The other is a VAT plate with an embedded rectangular delamination, as shown in Fig. 1 (c). The VAT plate is simply supported or clamped at all four edges, given by

$$w_0 = 0 \quad \text{at } x = \pm a/2, y = \pm b/2 \quad (\text{simply supported}) \quad (7a)$$

$$w_0 = 0, \frac{\partial w_0}{\partial x} = 0 \quad \text{at } x = \pm a/2 \quad (\text{clamped}) \quad (7b)$$

$$w_0 = 0, \frac{\partial w_0}{\partial y} = 0 \quad \text{at } y = \pm b/2$$

Moreover, the kinematic continuity conditions at the intersection of the undelaminated portion and each delaminated portion also need to be satisfied. In the prebuckling analysis, the kinematic continuity conditions of the delaminated VAT beam-plate or plate, without loss of generality, are expressed as

$$\begin{aligned}
u_0 = u_L, \quad \frac{\partial u_0}{\partial x} = \frac{\partial u_L}{\partial x}, \quad \frac{\partial u_0}{\partial y} = \frac{\partial u_L}{\partial y} \\
v_0 = v_L, \quad \frac{\partial v_0}{\partial x} = \frac{\partial v_L}{\partial x}, \quad \frac{\partial v_0}{\partial y} = \frac{\partial v_L}{\partial y}
\end{aligned} \quad (L=1,2) \quad (8)$$

Eq. (8) ensures the continuity of the in-plane displacements and strains at the intersection of the undelaminated portion and each delaminated portion. Note that, the in-plane displacements u_L and v_L of the L^{th} delaminated portion ($L=1, 2$) along the delamination edge are induced by the translational motion of the undelaminated portion. The continuity conditions along the edges between the non-delaminated portion and each delaminated portion must be enforced in the buckling model. If the delamination buckling problem is solved in a strong form [9, 10], both the kinematic continuity conditions and the continuity in moments and forces must be ensured. Since this work is applying the energy method in a weak form, only the kinematic continuity conditions need to be considered, as expressed by

$$w_0 = w_L, \quad \frac{\partial w_0}{\partial x} = \frac{\partial w_L}{\partial x}, \quad \frac{\partial w_0}{\partial y} = \frac{\partial w_L}{\partial y} \quad (L=1,2) \quad (9a)$$

$$u_L = -z_L \frac{\partial w_0}{\partial x}, \quad v_L = -z_L \frac{\partial w_0}{\partial y} \quad (L=1,2) \quad (9b)$$

where z_L is the position of the mid-plane of the L^{th} delaminated portion with respect to the reference plane along the thickness direction. The terms $-z_L w_{0,x}$ and $-z_L w_{0,y}$ in Eq. (9b) represent the in-plane displacements of the L^{th} delaminated portion ($L=1, 2$) along the delamination edge, which are generated by the rotation of transverse normal of the undelaminated portion, as illustrated by the right-hand plot in Fig. 2. These in-plane displacements result in an additional contribution of stretching energy to the delamination buckling analysis. If the kinematic continuity conditions in Eq. (9b) are not satisfied, the critical buckling load should be considerably underestimated.

4 Rayleigh-Ritz solution

4.1 Non-uniform in-plane stress distribution

Unlike constant stiffness laminated plates, VAT composite plates inevitably generate non-uniform in-plane stress distribution even when subjected to a simple uniform axial compression, either displacement-controlled or load-controlled [2, 3, 7]. Accordingly, it is necessary to perform a prebuckling analysis to determine the non-uniform in-plane stress distribution before buckling analysis. As mentioned earlier, the transverse edges are allowed to deform freely such that the edges ($y=\pm b/2$) are stress free, that is, $\bar{N}_{yy}=0, \bar{N}_{yx}=0$. Therefore, the total potential energy Π_p of the delaminated VAT plate under axial compression loading with transverse edges free to deform can be expressed as follows

$$\Pi_P = \Pi_S - \int_{\Gamma} (\bar{N}_{xx} u_0 + \bar{N}_{xy} v_0) dy \quad (10)$$

where Γ denotes the boundary edges, that is, $x=\pm a/2$. Π_S is the elastic strain energy of the delaminated VAT plate, which can be expanded into

$$\begin{aligned} \Pi_S = \frac{1}{2} \sum_{L=0}^2 \iint_{\Omega_L} & \left[A_{11}^L \left(\frac{\partial u_L}{\partial x} \right)^2 + 2A_{12}^L \left(\frac{\partial u_L}{\partial x} \right) \left(\frac{\partial v_L}{\partial y} \right) + 2A_{16}^L \left(\frac{\partial u_L}{\partial x} \right) \left(\frac{\partial u_L}{\partial y} + \frac{\partial v_L}{\partial x} \right) \right. \\ & \left. + 2A_{26}^L \left(\frac{\partial v_L}{\partial y} \right) \left(\frac{\partial u_L}{\partial y} + \frac{\partial v_L}{\partial x} \right) + A_{22}^L \left(\frac{\partial v_L}{\partial y} \right)^2 + A_{66}^L \left(\frac{\partial u_L}{\partial y} + \frac{\partial v_L}{\partial x} \right)^2 \right] dx dy \end{aligned} \quad (11)$$

with the integral area Ω_L of the L^{th} portion. The terms \bar{N}_{xx} and \bar{N}_{xy} are the boundary forces on the edges ($x=\pm a/2$). In the current work, each portion of the delaminated VAT plate is assumed to be balanced such that no extension-shear coupling exists, that is, $A_{16}^L = 0, A_{26}^L = 0$ [30]. Therefore, only the boundary force \bar{N}_{xx} on the edges ($x=\pm a/2$) is taken into account, even if the delaminated VAT plate is loaded by uniform axial compression [3, 7].

The Rayleigh-Ritz approach is then employed to solve the prebuckling problem in Eq. (10). The in-plane displacement fields of the delaminated VAT composite plate are expressed as

$$u_0(\xi, \eta) = \sum_{r=0}^R \sum_{s=0}^S U_{rs}^0 L_r(\xi) L_s(\eta), \quad v_0(\xi, \eta) = \sum_{r=0}^R \sum_{s=0}^S V_{rs}^0 L_r(\xi) L_s(\eta) \quad (12a)$$

$$\begin{aligned} u_L(\xi, \eta) &= \sum_{r=0}^R \sum_{s=0}^S U_{rs}^0 L_r(\xi) L_s(\eta) + \sum_{p=0}^P \sum_{q=0}^Q U_{pq}^L \phi_{pq}^u(\xi, \eta) \\ v_L(\xi, \eta) &= \sum_{r=0}^R \sum_{s=0}^S V_{rs}^0 L_r(\xi) L_s(\eta) + \sum_{p=0}^P \sum_{q=0}^Q V_{pq}^L \phi_{pq}^v(\xi, \eta) \end{aligned} \quad (L = 1, 2) \quad (12b)$$

where $\xi = 2x/a, \eta = 2y/b$. $L_r(\xi)$ and $L_s(\eta)$ are the r^{th} and s^{th} Legendre polynomials with respect to ξ and η , respectively. The terms U_{rs}^0 and V_{rs}^0 are the unknown coefficients of global shape functions, whereas the terms U_{pq}^L and V_{pq}^L are the unknown coefficients of local shape functions. The global shape functions in Eq. (12a) are incorporated into Eq. (12b) and the terms $\phi_{pq}^u(\xi, \eta)$ and $\phi_{pq}^v(\xi, \eta)$ in Eq. (12b) are assumed to be the local shape functions with null values outside the delamination region. As such, the kinematic continuity conditions in Eq. (8) are fully satisfied. For VAT composite plates with an embedded rectangular delamination, the local shape functions can be expressed as

$$\phi_{pq}^u(\xi, \eta) = (\beta_1^2 - \xi^2)^2 (\beta_2^2 - \eta^2)^2 L_p(\xi) L_q(\eta)$$

$$\phi_{pq}^v(\xi, \eta) = (\beta_1^2 - \xi^2)^2 (\beta_2^2 - \eta^2)^2 L_p(\xi) L_q(\eta)$$

Of special importance, the local shape functions corresponding to the through-the-width delamination are given by

$$\phi_p^u(\xi, \eta) = (\beta - \xi^2)^2 (1 - \eta^2)^2 L_p(\xi)$$

$$\phi_p^v(\xi, \eta) = (\beta - \xi^2)^2 (1 - \eta^2)^2 L_p(\xi)$$

where $\beta_1 = c/a, \beta_2 = c/b$.

Substituting the assumed in-plane displacement fields into Eq. (10), performing the necessary calculation of differentiation and integration, and minimize the resulting total potential energy Π_p with respect to the unknown coefficients, a set of linear algebraic equations in terms of unknown coefficients can be generated and written in the following matrix form

$$\mathbf{K}^m \mathbf{U} = \mathbf{F} \quad (13)$$

where \mathbf{K}^m is the membrane stiffness matrix of the delaminated VAT plate; \mathbf{U} the vector of the undetermined coefficients, that is, $\mathbf{U} = \{\mathbf{U}_{rs}^0 \quad \mathbf{V}_{rs}^0 \quad \mathbf{U}_{pq}^1 \quad \mathbf{V}_{pq}^1 \quad \mathbf{U}_{pq}^2 \quad \mathbf{V}_{pq}^2\}^T$. The vector \mathbf{F} is associated with prescribed axial compression loading. However, the prebuckling model given by Eq. (13) cannot be directly applied to analyze the prebuckling problem of the VAT plate under a uniform displacement loading, as denoted in Fig. 1 (b) and (c) and expressed in Eq. (5b). The primary reason is that the boundary force \bar{N}_{xx} on the edges ($x=\pm a/2$) of the delaminated VAT plate corresponding to uniform axial compression is unknown and needs to be determined. To address this problem, Wu and co-workers [3, 6] proposed that the prebuckling problem of the VAT plate under uniform axial compression can be modelled as a superposition of the VAT plate under the action of a series of prescribed compression loadings, expressed as

$$\bar{N}_{xx}(\eta) = \sum_{j=1}^J C_j L_j(\eta) \quad (14)$$

where C_j is the unknown coefficients to be determined. $L_j(\eta)$ is the j^{th} boundary force on the edges ($x=\pm a/2$), represented by the j^{th} Legendre polynomial. Therefore, the resulting equation governing the prebuckling problem of the delaminated VAT plate loaded by uniform axial compression is rewritten as

$$\mathbf{K}^m \mathbf{U} = \sum_j C_j \mathbf{F}_j \quad (15)$$

where the vector \mathbf{F}_j is associated with the j^{th} axial compression loading, namely, $L_j(\eta)$. The end-shortening value corresponding to the j^{th} boundary force is then determined by the following expression [6]

$$\Xi_j(\eta) = u_0(1, \eta) - u_0(-1, \eta) \quad (16)$$

Once this procedure is done, the unknown coefficients C_j are determined from a set of control points for the function $\Xi_j(\eta)$ with the given uniform end-shortening value Δ [3]. With the solution of the in-plane displacement fields given by Eq. (15), the non-uniform in-plane stress resultants of the delaminated VAT plate under uniform axial compression can be determined from a modified version of Eq. (2).

4.2 Buckling analysis

The buckling model for delaminated VAT plates is also derived from the principle of minimum potential energy and the Rayleigh-Ritz approach. The total potential energy Π of the delaminated VAT plate in its buckled shape can be expressed as

$$\Pi = U + V \quad (17)$$

where V is the external work of the applied load; U is the total strain energy of the delaminated VAT panel, which can be expressed as

$$U = \sum_{L=0}^2 U_b^L + \sum_{L=1}^2 U_{in}^L \quad (18)$$

where U_b^L is the bending energy term for the L^{th} portion ($L=0,1,2$) and U_{in}^L the in-plane strain energy of the L^{th} delaminated portion ($L=1, 2$). In expanded form, these terms become

$$U_b^L = \frac{1}{2} \iint_{\Omega_L} \left[D_{11}^L \left(\frac{\partial^2 w_L}{\partial x^2} \right)^2 + 2D_{12}^L \left(\frac{\partial^2 w_L}{\partial x^2} \right) \left(\frac{\partial^2 w_L}{\partial y^2} \right) + 4D_{66}^L \left(\frac{\partial^2 w_L}{\partial x \partial y} \right) \left(\frac{\partial^2 w_L}{\partial x \partial y} \right) + D_{22}^L \left(\frac{\partial^2 w_L}{\partial y^2} \right)^2 + 4D_{16}^L \left(\frac{\partial^2 w_L}{\partial x^2} \right) \left(\frac{\partial^2 w_L}{\partial x \partial y} \right) + 4D_{26}^L \left(\frac{\partial^2 w_L}{\partial y^2} \right) \left(\frac{\partial^2 w_L}{\partial x \partial y} \right) \right] dx dy \quad (19a)$$

$$U_{in}^L = \frac{1}{2} \iint_{\Omega_L} \left[A_{11}^L \left(\frac{\partial u_L}{\partial x} \right)^2 + 2A_{12}^L \left(\frac{\partial u_L}{\partial x} \right) \left(\frac{\partial v_L}{\partial y} \right) + 2A_{16}^L \left(\frac{\partial u_L}{\partial x} \right) \left(\frac{\partial u_L}{\partial y} + \frac{\partial v_L}{\partial x} \right) + 2A_{26}^L \left(\frac{\partial v_L}{\partial y} \right) \left(\frac{\partial u_L}{\partial y} + \frac{\partial v_L}{\partial x} \right) + A_{22}^L \left(\frac{\partial v_L}{\partial y} \right)^2 + A_{66}^L \left(\frac{\partial u_L}{\partial y} + \frac{\partial v_L}{\partial x} \right)^2 \right] dx dy \quad (19b)$$

As also illustrated in Fig. 2, the rotation of transverse normal of the undelaminated portion along the delamination edges eventually leads to the staggered forms of in-plane motion of each delaminated portion. Such in-plane deformations generates additional strain energy U_{in}^L , which is stored in the L^{th} delaminated portion ($L=1,2$). From the energetic point of view, the additional in-plane strain energy U_{in}^L of the L^{th} delaminated portion can be considered as a compensation for the partial loss of the original bending energy U_b^0 of the undelaminated portion. Therefore, the in-plane strain energy U_{in}^L stored in the L^{th} delaminated portion is essential for the buckling analysis of delaminated VAT plates.

The external work V of the in-plane stress resultants obtained in the prebuckling analysis is given by

$$V = \sum_{L=0}^2 V_p^L \quad (20)$$

where V_p^L is the external work of the L^{th} portion, expressed as

$$V_p^L = \frac{1}{2} \lambda \iint_{\Omega_L} \left[N_{xx}^L \left(\frac{\partial w_L}{\partial x} \right)^2 + N_{yy}^L \left(\frac{\partial w_L}{\partial y} \right)^2 + 2N_{xy}^L \left(\frac{\partial w_L}{\partial x} \right) \left(\frac{\partial w_L}{\partial y} \right) \right] dx dy \quad (21)$$

The Rayleigh-Ritz approach is then applied to solve the buckling problem of the

delaminated VAT composite plates, expressed in Eq. (17). Applying the superposition method, the assumed displacement fields are constructed from the global shape functions, which satisfy the geometric boundary conditions in Eq. (6) or Eq. (7), and local shape functions, which are analogous to clamped boundary conditions along the delamination edges. In doing so, the kinematical continuity condition of Eq. (9) can be satisfied. The displacement fields of the delaminated VAT composite plate can be expressed as

$$w_0 = \sum_{m=0}^M \sum_{n=0}^N W_{mn}^0 X_m^w(\xi) Y_n^w(\eta) \quad (22a)$$

$$w_L = \sum_{m=0}^M \sum_{n=0}^N W_{mn}^0 X_m^w(\xi) Y_n^w(\eta) + \sum_{\bar{m}=0}^{\bar{M}} \sum_{\bar{n}=0}^{\bar{N}} W_{\bar{m}\bar{n}}^L \psi_{\bar{m}\bar{n}}^w(\xi, \eta) \quad (22b)$$

$$u_L = \sum_{p=0}^P \sum_{q=0}^Q \tilde{U}_{pq}^L \psi_{pq}^u(\xi, \eta) - z_L \sum_{m=0}^M \sum_{n=0}^N W_{mn}^0 g_{mn}(\xi, \eta) \quad (22c)$$

$$v_L = \sum_{p=0}^P \sum_{q=0}^Q \tilde{V}_{pq}^L \psi_{pq}^v(\xi, \eta) - z_L \sum_{m=0}^M \sum_{n=0}^N W_{mn}^0 h_{mn}(\xi, \eta) \quad (22d)$$

where W_{mn}^0 , $W_{\bar{m}\bar{n}}^L$, \tilde{U}_{pq}^L and \tilde{V}_{pq}^L are the undetermined coefficients. The term $X_m^w(\xi)Y_n^w(\eta)$ is the global shape function for the out-of-plane displacements. The terms $\psi_{\bar{m}\bar{n}}^w(\xi, \eta)$, $\psi_{pq}^u(\xi, \eta)$ and $\psi_{pq}^v(\xi, \eta)$ denote the local shape functions with null values outside the delamination region. With Eqs. (22a) and (22b), the kinematic continuity conditions in Eq. (9a) are satisfied during the buckling analysis. Moreover, the terms $-z_L W_{mn}^0 g_{mn}(\xi, \eta)$ and $-z_L W_{mn}^0 h_{mn}(\xi, \eta)$ are introduced to satisfy the kinematic continuity conditions in Eq. (9b). The additional shape functions $g_{mn}(\xi, \eta)$ and $h_{mn}(\xi, \eta)$ can be constructed approximately in many different ways provided that the kinematic continuity conditions in Eq. (9b) are satisfied along the delamination edges. In the present work, the linear interpolation method is used. For a VAT plate with a through-the-width delamination, both global and local shape functions are expressed as

$$X_m^w(\xi)Y_n^w(\eta) = (1 - \xi^2)L_m(\xi)L_n(\eta)$$

$$\psi_{\bar{m}\bar{n}}^w(\xi, \eta) = \beta_1^2 - \xi^2 \quad \delta_{\bar{m}\bar{n}}(\xi, \eta)$$

$$\psi_{pq}^u(\xi, \eta) = \psi_{pq}^v(\xi, \eta) = (\beta_1^2 - \xi^2)^2 (1 - \eta^2)^2 L_p(\xi)L_q(\eta)$$

$$g_{mn}(\xi, \eta) = X_{m,\xi}^w(-\beta_1)Y_n^w(\eta) \frac{\beta_1 - \xi}{2\beta_1} + X_{m,\xi}^w(\beta_1)Y_n^w(\eta) \frac{\beta_1 + \xi}{2\beta_1}$$

$$h_{mn}(\xi, \eta) = X_m^w(-\beta_1)Y_{n,\eta}^w(\eta) \frac{\beta_1 - \xi}{2\beta_1} + X_m^w(\beta_1)Y_{n,\eta}^w(\eta) \frac{\beta_1 + \xi}{2\beta_1}$$

For a VAT plate with an embedded rectangular delamination, both global and local shape functions are given by

$$X_m^w(\xi)Y_n^w(\eta) = (1 - \xi^2)(1 - \eta^2)L_m(\xi)L_n(\eta)$$

$$\psi_{\bar{m}\bar{n}}^w(\xi, \eta) = (\beta_1^2 - \xi^2)^2 (\beta_2^2 - \eta^2)^2 L_{\bar{m}}(\xi) L_{\bar{n}}(\eta)$$

$$\psi_{pq}^u(\xi, \eta) = \psi_{pq}^v(\xi, \eta) = (\beta_1^2 - \xi^2)^2 (\beta_2^2 - \eta^2)^2 L_p(\xi) L_q(\eta)$$

$$g_{mn}(\xi, \eta) = X_{m,\xi}^w(-\beta_1) Y_n^w(\eta) \frac{\beta_1 - \xi}{2\beta_1} + X_{m,\xi}^w(\beta_1) Y_n^w(\eta) \frac{\beta_1 + \xi}{2\beta_1}$$

$$h_{mn}(\xi, \eta) = X_m^w(\xi) Y_{n,\eta}^w(-\beta_2) \frac{\beta_2 - \eta}{2\beta_2} + X_m^w(\xi) Y_{n,\eta}^w(\beta_2) \frac{\beta_2 + \eta}{2\beta_2}$$

Substituting the assumed displacement fields and the in-plane stress resultants into Eq. (17), and minimizing the total potential energy Π , a set of algebraic equations is then obtained and expressed in the following matrix form,

$$(\mathbf{K} + \lambda \mathbf{L}) \mathbf{A} = \mathbf{0} \quad (23)$$

where \mathbf{K} is the bending stiffness matrix of the delaminated VAT plate; \mathbf{L} is the stability matrix due to the in-plane stress resultants distribution obtained in the prebuckling analysis; λ is the eigenvalue; \mathbf{A} is the vector of unknown coefficients of all the shape functions, that is, $\mathbf{A} = \{\mathbf{U}_{pq}^1 \quad \mathbf{V}_{pq}^1 \quad \mathbf{U}_{pq}^2 \quad \mathbf{V}_{pq}^2 \quad \mathbf{W}_{mn}^0 \quad \mathbf{W}_{mn}^1 \quad \mathbf{W}_{mn}^2\}^T$. The resulting matrices \mathbf{K} and \mathbf{L} can be expanded into,

$$\mathbf{K} = \begin{bmatrix} \mathbf{K}_{U_1 U_1} & \mathbf{K}_{U_1 V_1} & \mathbf{0} & \mathbf{0} & \mathbf{K}_{U_1 W_0} & \mathbf{0} & \mathbf{0} \\ \mathbf{K}_{V_1 U_1} & \mathbf{K}_{V_1 V_1} & \mathbf{0} & \mathbf{0} & \mathbf{K}_{V_1 W_0} & \mathbf{0} & \mathbf{0} \\ \mathbf{0} & \mathbf{0} & \mathbf{K}_{U_2 U_2} & \mathbf{K}_{U_2 V_2} & \mathbf{K}_{U_2 W_0} & \mathbf{0} & \mathbf{0} \\ \mathbf{0} & \mathbf{0} & \mathbf{K}_{V_2 U_2} & \mathbf{K}_{V_2 V_2} & \mathbf{K}_{V_2 W_0} & \mathbf{0} & \mathbf{0} \\ \mathbf{K}_{W_0 U_1} & \mathbf{K}_{W_0 V_1} & \mathbf{K}_{W_0 U_2} & \mathbf{K}_{W_0 V_2} & \mathbf{K}_{W_0 W_0} & \mathbf{K}_{W_0 W_1} & \mathbf{K}_{W_0 W_2} \\ \mathbf{0} & \mathbf{0} & \mathbf{0} & \mathbf{0} & \mathbf{K}_{W_1 W_0} & \mathbf{K}_{W_1 W_1} & \mathbf{0} \\ \mathbf{0} & \mathbf{0} & \mathbf{0} & \mathbf{0} & \mathbf{K}_{W_2 W_0} & \mathbf{0} & \mathbf{K}_{W_2 W_2} \end{bmatrix}$$

$$\mathbf{L} = \begin{bmatrix} \mathbf{0} & \mathbf{0} & \mathbf{0} & \mathbf{0} & \mathbf{0} & \mathbf{0} & \mathbf{0} \\ \mathbf{0} & \mathbf{0} & \mathbf{0} & \mathbf{0} & \mathbf{0} & \mathbf{0} & \mathbf{0} \\ \mathbf{0} & \mathbf{0} & \mathbf{0} & \mathbf{0} & \mathbf{0} & \mathbf{0} & \mathbf{0} \\ \mathbf{0} & \mathbf{0} & \mathbf{0} & \mathbf{0} & \mathbf{0} & \mathbf{0} & \mathbf{0} \\ \mathbf{0} & \mathbf{0} & \mathbf{0} & \mathbf{0} & \mathbf{L}_{W_0 W_0} & \mathbf{L}_{W_0 W_1} & \mathbf{L}_{W_0 W_2} \\ \mathbf{0} & \mathbf{0} & \mathbf{0} & \mathbf{0} & \mathbf{L}_{W_1 W_0} & \mathbf{L}_{W_1 W_1} & \mathbf{0} \\ \mathbf{0} & \mathbf{0} & \mathbf{0} & \mathbf{0} & \mathbf{L}_{W_2 W_0} & \mathbf{0} & \mathbf{L}_{W_2 W_2} \end{bmatrix}$$

The terms associated with the vector $\{\mathbf{U}_{pq}^1 \quad \mathbf{V}_{pq}^1 \quad \mathbf{U}_{pq}^2 \quad \mathbf{V}_{pq}^2\}^T$ in the elastic stiffness matrix are derived from the second part on the right hand side of Eq. (18). Therefore, it can be derived that the vector $\{\mathbf{U}_{pq}^1 \quad \mathbf{V}_{pq}^1 \quad \mathbf{U}_{pq}^2 \quad \mathbf{V}_{pq}^2\}^T$ can be represented linearly in terms of the vector $\{\mathbf{W}_{mn}^0\}^T$. This consideration further shows that the in-plane deformations of both upper and lower delaminated portions are induced by the out-of-plane deformation of the undelaminated portion. Therefore, Eq. (23) can be reduced to

$$(\tilde{\mathbf{K}} + \lambda \tilde{\mathbf{L}})\Theta = \mathbf{0} \quad (24)$$

where $\Theta = \{\mathbf{W}_{mn}^0 \quad \mathbf{W}_{mn}^1 \quad \mathbf{W}_{mn}^2\}^T$, and the matrices $\tilde{\mathbf{K}}$ and $\tilde{\mathbf{L}}$ are rewritten as,

$$\tilde{\mathbf{K}} = \begin{bmatrix} \mathbf{K}_{w_0 w_0} - \hat{\mathbf{K}}_{w_0 w_0} & \mathbf{K}_{w_0 w_1} & \mathbf{K}_{w_0 w_2} \\ \mathbf{K}_{w_1 w_0} & \mathbf{K}_{w_1 w_1} & \mathbf{0} \\ \mathbf{K}_{w_2 w_0} & \mathbf{0} & \mathbf{K}_{w_2 w_2} \end{bmatrix}, \quad \tilde{\mathbf{L}} = \begin{bmatrix} \mathbf{L}_{w_0 w_0} & \mathbf{L}_{w_0 w_1} & \mathbf{L}_{w_0 w_2} \\ \mathbf{L}_{w_1 w_0} & \mathbf{L}_{w_1 w_1} & \mathbf{0} \\ \mathbf{L}_{w_2 w_0} & \mathbf{0} & \mathbf{L}_{w_2 w_2} \end{bmatrix}$$

$$\hat{\mathbf{K}}_{w_0 w_0} = \left[\mathbf{K}_{w_a u} \quad \mathbf{K}_{w_a v} \quad \mathbf{K}_{w_u} \quad \mathbf{K}_{w_v} \right] \begin{bmatrix} \mathbf{K}_{u_1 u_1} & \mathbf{K}_{u_1 v_1} & \mathbf{0} & \mathbf{0} \\ \mathbf{K}_{v_1 u_1} & \mathbf{K}_{v_1 v_1} & \mathbf{0} & \mathbf{0} \\ \mathbf{0} & \mathbf{0} & \mathbf{K}_{u_2 u_2} & \mathbf{K}_{u_2 v_2} \\ \mathbf{0} & \mathbf{0} & \mathbf{K}_{v_2 u_2} & \mathbf{K}_{v_2 v_2} \end{bmatrix}^{-1} \begin{bmatrix} \mathbf{K}_{u_1 v} \\ \mathbf{K}_{v_1 v} \\ \mathbf{K}_{u_2 v} \\ \mathbf{K}_{v_2 v} \end{bmatrix}$$

The lowest eigenvalue λ_{cr} obtained from Eq. (24) corresponds to the end-shortening strain under the critical buckling state. Combined with Eqs. (22a) and (22b), the buckling mode shapes of both upper and lower sublaminates can be obtained using the vector $\Theta = \{\mathbf{W}_{mn}^0 \quad \mathbf{W}_{mn}^1 \quad \mathbf{W}_{mn}^2\}^T$. The average critical buckling load of the delaminated VAT plate is evaluated by the following expression [2, 3, 7],

$$N_x^{cr} = \frac{\lambda_{cr}}{b} \int_{-b/2}^{b/2} N_{xx}^0(a/2, y) dy \quad (25)$$

4.3 Contact problem

In view of Eq. (24), both upper and lower delaminated portions within the delamination region deform freely without touching each other, and thus have independent transverse deformations. As such, the model described above is referred to as ‘*free mode*’ model, which can readily capture the delamination opening. However, for an off-midplane delamination, in particular a near-surface debonded layer, the buckling mode shape obtained by Eq. (24) could be physically inadmissible [14, 19, 32]. In this case, the two delaminated portions interpenetrate with each other and the contact problem must be considered in the delamination buckling analysis. Indeed, under these circumstances, the penetration of the thinner delaminated portion is prevented by the thicker delaminated portion, and eventually both of delaminated portions buckle in a constrained mode shape. Shu [14] proposed a ‘*totally constrained mode*’ model to avoid this contact problem. In this method, the delaminated portions are constrained to undergo identical transverse displacements, that is $w_1 = w_2$ etc. Note, for the cases when contact occurs, the ‘*free mode*’ model given by Eq. (24) and Shu’s ‘*totally constrained mode*’ model provide lower and upper bounds for the critical delamination buckling load prediction, respectively [14].

In most cases, however, the buckled state is partially constrained at the delamination interface when contact buckling occurs. A nonlinear elastic foundation was introduced by Shahwan and Waas [20] to conduct the contact buckling analysis for the debonded

near-surface layer partially constrained by the presence of a rigid surface. However, the resulting nonlinear equations need to be solved, which introduce complications that are associated with the foundation's force-displacement relationship. An alternative approach to address this contact problem is the constrained point/area method [25, 32, 33]. In the current work, the constrained point method [32, 33] is employed and extended to consider the contact effects in the delamination buckling analysis. The main advantage of this approach is that if the constrained points are selected appropriately, the buckling load and its corresponding constrained mode shape can be readily obtained from a normal eigenvalue analysis with an improved version of Eq. (24). In this method, the contact area is assumed to be small compared with the delaminated area and the delaminated composite plate is rigid in the thickness direction. Under these circumstances, the delaminated portions touch each other at some appropriate contact points. Subsequently, a virtual spring with translational (K_0) and rotational (K_1 and K_2) stiffness is assumed to apply at each potential contact point, where the reaction force (P_0) and moments (M_1 and M_2) are given as [32, 33],

$$P_0 = -K_0(w_1 - w_2) \quad (26a)$$

$$M_1 = -K_1(w_{1,x} - w_{2,x}) \quad (26b)$$

$$M_2 = -K_2(w_{1,y} - w_{2,y}) \quad (26c)$$

The spring stiffness values (K_0 , K_1 and K_2) can be determined from the elastic properties of the plates [32, 33]. When contact buckling occurs, the energy stored in the virtual spring is expressed as

$$U_{\text{cons}} = \frac{1}{2} \sum_{i=1}^I \{ K_0 [w_1(x_i, y_i) - w_2(x_i, y_i)]^2 + K_1 [w_{1,x}(x_i, y_i) - w_{2,x}(x_i, y_i)]^2 + K_2 [w_{1,y}(x_i, y_i) - w_{2,y}(x_i, y_i)]^2 \} \quad (27)$$

where (x_i, y_i) represents the i^{th} constrained point. By differentiating Eq. (27) with respect to the generalized coordinates ($\Theta = \{\mathbf{W}_{\text{mn}}^0 \quad \mathbf{W}_{\text{mn}}^1 \quad \mathbf{W}_{\text{mn}}^2\}^T$), an additional stiffness matrix is obtained as

$$\tilde{\mathbf{K}}_{\text{cons}} = \sum_{i=1}^I \begin{bmatrix} \mathbf{K}_{w_0 w_0}^{(i)} & \mathbf{K}_{w_0 w_1}^{(i)} & \mathbf{K}_{w_0 w_2}^{(i)} \\ \mathbf{K}_{w_1 w_0}^{(i)} & \mathbf{K}_{w_1 w_1}^{(i)} & \mathbf{K}_{w_1 w_2}^{(i)} \\ \mathbf{K}_{w_2 w_0}^{(i)} & \mathbf{K}_{w_2 w_1}^{(i)} & \mathbf{K}_{w_2 w_2}^{(i)} \end{bmatrix} \quad (28)$$

Eq. (28) is then inserted into the bending stiffness matrix $\tilde{\mathbf{K}}$ of Eq. (24). As such, the contact effects at the constrained points are included.

A constrained-point-searching procedure is required to ensure that all of the constrained moments are zero and no interpenetration occurs at the actual constrained points. Firstly, the buckling analysis is performed on the 'free mode' model described by Eq. (24). The critical buckling mode shape is then examined to whether it is physically admissible or not. If the initially obtained mode shape is not admissible, a constrained point is applied at the centre of

an interpenetrated area. Subsequently, Eq. (24) is augmented to take into account the contact effects at constrained points and solved again. The contact point is moved by Δx and Δy as given by [32],

$$\Delta x = s_1 M_1 / P_0 \quad (29a)$$

$$\Delta y = s_2 M_2 / P_0 \quad (29b)$$

where s_1 and s_2 are constants that are determined according to the state of the convergence [32]. The procedure is repeated until the movements Δx and Δy become sufficiently small (i.e. tolerance less than 10^{-4} is used in this work). Finally, the buckling load and its corresponding constrained mode shape are determined after the location of the contact point is decided.

5 Results and Discussion

This section presents a detailed study on the buckling behaviour of VAT composite plates with a single rectangular delamination under uniform axial compression. The VAT composite plates considered are square in shape, that is, $a=b=0.81408\text{m}$. The lamina properties for the graphite-epoxy composite are $E_{11}=181\text{GPa}$, $E_{22}=10.3\text{GPa}$, $G_{12}=7.17\text{GPa}$ and $\nu_{12}=0.28$ with ply thickness equal to be 0.127mm . To validate the present analytical method, the finite-element model using the commercial package Abaqus is also implemented for the delamination buckling analysis of VAT laminates. A subroutine is developed to generate the composite element with independent fibre orientations. The SC8R shell element is chosen for both prebuckling and buckling analysis of the delaminated VAT plate and very fine meshes are used to achieve the desired accuracy. In the FEM model, the VAT plate is split into two parts, representing the upper and lower sublaminates. Then, the nodal displacements of two adjacent surfaces of the two sublaminates over the undelaminated region are tied using multi-point constraints (MPCs). In addition, to facilitate the comparison of the numerical results on delamination buckling, the delamination position (h_1), length (c) and area (c^2) are normalized with respect to the plate thickness (h_0), plate length (a) and plate area ($a \times b$), respectively. The following three parameters are used in the following analysis: the normalized delamination position h_1/h ; the normalized delamination length c/a and the normalized delamination area c^2/ab .

5.1 Convergence study and model validation

To perform the convergence study, a constant stiffness plate with the layup $[0]_{20}$ and a through-the-width delamination under in-plane axial compression is considered in this section. The loading edges of this plate are clamped and the other two edges are free (CFCF), which is analogous to the beam-plate analyzed in Simitse et al. [9]. In this study, the through-the-width delamination parameters of h_1/h and c/a are taken to be 0.5 and 0.6, respectively. The present analytical modelling is applied to determine the critical buckling load of the delaminated plate

$[0]_{20}$ using different number of terms (3 ~ 9) for the global and local shape functions. The critical buckling load of the delaminated plate is normalized with respect to that of an intact plate. Table 1 presents the normalized critical buckling loads of the delaminated plate $[0]_{20}$ obtained using different number of shape-function terms. The results obtained using FEM and those in the previous works by Simitsets et al. [9] and Lee et al. [12] are included for comparison purposes. As shown in Table 1, the results predicted by the present analytical model match closely with results given by FEM and previous works. It was found that five terms for the global and local shape functions are sufficient to yield accurate results. However, the FEM requires very fine meshes, $60 \times 60 \times 20$, to reach the desired accuracy of results.

To further validate the present delamination buckling model, buckling analysis is also performed on a delaminated composite plate $[0]_{20}$ with two opposite edges simply-supported and the other two edges free (SFSF). In this case study, the normalized delamination position h_1/h and length c/a of the through-the-width delamination are chosen to be 0.4 and five different values (0.0, 0.2, 0.4, 0.6, and 0.8), respectively. The normalized critical buckling loads obtained by the present method for this case study are shown in Table 2 and compared with the results previously published by Simitsets et al. [9] and Shu [14]. Table 2 shows a good agreement for the normalized critical buckling loads between the present method, the FEM and the previous published results.

More numerical results on the normalized critical buckling load of the delaminated composite plate $[0]_{20}$ with SFSF and CFCF boundary conditions are obtained and shown in Table 3. Three different delamination positions ($h_1/h=0.1, 0.3$ and 0.5) are considered, and the normalized length c/a of the delamination vary from 0 to 0.9 with 0.1 increment. The numerical results obtained using the analytical model in Table 3 have shown a good agreement with the results given by Simitsets et al. [9], which further approves the proposed analytical method for the delamination buckling analysis.

5.2 Residual buckling load of delaminated plates

This section presents the numerical study on the buckling behaviour of the angle-ply laminated plates and the VAT composite plates with a through-the-width delamination or an embedded rectangular delamination. In the through-the-width delamination study, the laminate layups $[\pm 45]_{4s}$ and $[\pm(0,30)]_{4s}$ with two different delamination positions of $h_1/h=0.25$ and 0.5 are considered. The normalized delamination length c/a varies from 0.0 to 0.9 with an incremental step of 0.1. Both $[\pm 45]_{4s}$ and $[\pm(0,30)]_{4s}$ layups exhibit a certain amount of bending-twisting coupling effects, and the in-plane stress fields of the VAT plate $[\pm(0,30)]_{4s}$ are highly non-uniform with the uniform axial compression loading. It was found that six Legendre polynomial terms in the expressions given by Eqs. (12) and (14) were used to ensure numerical precision in the prebuckling analysis. Tables 4 and 5 show the numerical

results on the normalized critical buckling loads for the angle-ply plate $[\pm 45]_{4s}$ and the VAT plate $[\pm(0,30)]_{4s}$ with a through-the-width delamination for a series of different combinations of h_1/h and c/a values. Tables 4 and 5 present the numerical results of the normalized delamination buckling load of the layups $[\pm 45]_{4s}$ and $[\pm(0,30)]_{4s}$, respectively, which are obtained by the analytical model with and without considering the in-plane strain energy terms in Eq. (18). It is noted that excellent agreement between the analytical and FEM results has been reached when the in-plane strain energy terms are included into the delamination buckling analysis. However, considerable errors are incurred to the prediction of critical delamination buckling loads if the in-plane energy terms are not taken into account. Therefore, considering the in-plane deformations of the delaminated portions within the delamination region that are generated by the rotation of transverse normal of the undelaminated portion along the delamination edge, is essential for the accurate computation of critical buckling loads of delaminated composite plates.

The buckling behaviour of composite laminated plates with an embedded rectangular delamination is also studied using the present analytical model. Herein, two different laminate layups $[\pm 45]_{4s}$ and $[\pm(0,90)]_{4s}$ are studied, and the composite plates are assumed to be simply supported at all four edges and is subjected to a uniform axial compression. In this case, two different delamination positions ($h_1/h=0.25$ or 0.5) are considered and the delamination size is characterized by the normalized delamination area c^2/ab ranging from 0.0 to 0.81. The in-plane stress fields of the VAT plate $[\pm(0,90)]_{4s}$ are also highly non-uniform with the uniform axial compression loading. Tables 6 and 7 present the numerical results of the normalized critical buckling loads of composite plates $[\pm 45]_{4s}$ and $[\pm(0,90)]_{4s}$ containing an embedded rectangular delamination with respect to a series of different combinations of h_1/h and c^2/ab values. The analytical results shown in Tables 6 and 7 closely match with FEM simulation results. Therefore, these observations further demonstrate the accuracy of this proposed analytical model for the delamination buckling analysis of both straight-fibre composite plates and VAT plates.

Subsequently, the numerical results for the VAT composite plate $[\pm(0,30)]_{4s}$ in Table 5 and the VAT plate $[\pm(0,90)]_{4s}$ in Table 7 are used to study the effects of delamination size and position on the residual buckling loads of delaminated VAT composite plates. To compare the results with respect to different composite layups, a buckling coefficient defined in previous works [2, 3, 7], as given by Eq. (30), is used to normalize the buckling load of the delaminated VAT plates.

$$K_{cr} = \frac{N_x^cr a^2}{E_{11} h^3} \quad (30)$$

The buckling coefficients of two delaminated composite plates $[\pm(0,30)]_{4s}$ and $[\pm(0,90)]_{4s}$ are then, respectively, plotted in Fig. 3 (a) and (b) with respect to the variation of the rectangular

delamination size (c/a for the through-the-width delamination and c^2/ab for the embedded delamination). In Fig. 3 (a) and (b), each curve represents a particular delamination position, namely, $h_1/h=0.25$ or 0.5 . At the initial stage when the delamination is small, the buckling coefficients remain almost unchanged for all the cases in Fig 3. Afterwards, the buckling loads of the VAT plates reduce when the delamination size gradually increases. It is also interesting to note that, for both delaminated VAT plates, the reduction of buckling loads with $h_1/h=0.25$ is much more prominent than that with $h_1/h=0.5$. This behaviour is expected because the delamination position h_1/h has a significant effect on the buckling behaviour of delaminated composite plates.

$h_1/h=0.5$ denotes a mid-plane delamination, and also indicates that the upper and lower sublaminates are identical. These two delaminated portions have the same amount of deformations when the critical buckling occurs, thus the plates do not open up at the delamination interface. In this case, the buckling load reduction of the delaminated composite plates is mainly attributed to the loss of bending stiffness within the delamination region. It becomes an off-midplane delamination when the delamination position $h_1/h=0.25$. For composite plates with an off-midplane delamination, the bending stiffness of the thinner delaminated portion within the delamination region is much less than that of the thicker one. As a result, the out-of-plane deformation of the thinner sublaminate is larger than that of the thicker sublaminate. With an increasing c/a value, the two sublaminates can separate physically and an opening mode is generated for the delaminated plates when buckling occurs. In some extreme cases, only the thinner sublaminate buckles, which forms a completely local buckling behaviour [16, 18]. Consequently, an off-midplane type of delamination can further aggravate the reduction of the critical buckling load of the delaminated composite plates.

5.3 Buckling mode shapes of delaminated VAT plates

The effects of the delamination size and position on the buckling mode shapes of the delaminated composite plates are studied in this section. The composite plate $[0]_{20}$ with a through-the-width delamination is considered first. The loading edges of this plate are simply supported and the other two edges are free (SFSF). Fig. 4 shows nine different cross sections of the buckling mode shapes of the delaminated plate $[0]_{20}$ along the x -axis ($y=0$) with respect to a series of different combinations of h_1/h and c/a values. When the delamination is relatively small ($c/a=0.1$) or the delamination interface is close to the mid-plane ($h_1/h=0.5$), the upper and lower sublaminates deform to the same shape, and result in a global buckling mode shape. This effect is clearly denoted by the three plots in the first column (for a small delamination size $c/a=0.1$) and the remaining three plots in the last row (for a mid-plane delamination $h_1/h=0.5$) of Fig. 4.

When the delamination is away the midplane and is also relatively large, the delaminated

portions do not deform to the same shape, and leads to the delamination opening up in the buckling mode shapes. Under such circumstances, the local buckling shapes or mixed buckling shapes appear to the delaminated composite plates when critical buckling occurs. The last two plots in the second row of Fig. 4 (with $h_1/h=0.3$, $c/a=0.5$ and 0.9) illustrate the case of combined buckling mode shapes, in which both the upper and lower sublaminates have a certain amount of deformations, but do not have the same shape. When one of the delaminated portions is thin ($h_1/h=0.1$) and the delamination size is relatively large, the local buckling mode shape of the thin sublaminate appears at relatively low buckling load (see Table 3). This local buckling behaviour of the delaminated composite plate is demonstrated in the last two plots ($h_1/h=0.1$, $c/a=0.5$ and 0.9) in the first row of Fig. 4.

Subsequently, the buckling mode shapes of the VAT plate $[\pm(0,30)]_{4s}$ in Table 5 and the VAT plate $[\pm(0,90)]_{4s}$ in Table 7 are studied. The buckling mode shapes of the delaminated VAT plates $[\pm(0,30)]_{4s}$ and $[\pm(0,90)]_{4s}$ with respect to different normalized delamination position/length and position/area combinations are shown in Figs. 5 and 6, respectively. The good agreement between the analytical and FEM results in Figs. 5 and 6, shows that the proposed analytical method is capable of accurately capturing the buckling mode shapes of the delaminated VAT plates. Compared with the above analysis with respect to the straight-fibre laminates $[0]_{20}$, similar conclusions are drawn from the buckling mode shapes of the delaminated VAT plate shown in Figs. 5 and 6.

When the delamination is at the mid-plane, that is, $h_1/h=0.5$, both upper and lower delaminated portions have the same bending stiffness within the delamination region, leading to the same tendency to deform without opening modes when critical buckling occurs. It therefore produces the global buckling mode shapes, as shown in the plots (with $h_1/h=0.5$) of Figs. 5 and 6. In this case, the buckling load reduction of the delaminated composite plates is mainly attributed to the loss of bending stiffness within the delamination region, as mentioned above. When the delamination is not located on the mid-plane ($h_1/h=0.25$) and the delamination is relatively large ($c/a=0.5$ or 0.9 in Fig. 5 and $c^2/ab=0.36$ or 0.81 in Fig. 6), the thinner delaminated portion of the VAT plate within the delamination region undergoes much larger deformation than the thicker one at the critical buckling point. As a consequence, the delamination opens up and the delaminated plate exhibits a mixed or local buckling mode shape, as denoted by the last two plots with $h_1/h=0.25$ in Figs. 5 and 6. The delamination opening leads to further reduction of the critical buckling load (as illustrated in Fig. 3 (a) and (b)).

For composite plates with a considerably large and off-midplane delamination, as shown in Figs. 4-6, most buckling mode shapes of the thinner delaminated portions are in the form of single half-waves. For these cases, no contact between the delaminated portions occurs and we can apply the 'free mode' model to predict the delamination buckling load. However, when the

buckling mode shape of the thinner delaminated portion is in the form of multiple half-waves, as shown in Figs. 7(a) and 8(a), the buckling mode shapes obtained using the ‘*free mode*’ model become physically inadmissible. Under such cases, the thinner delaminated portion rests on the thicker delamination portion, and thus contact buckling may occur [19, 20, 32, 33]. Therefore, we need to apply the ‘*constrained mode*’ model to take into account the contact effects at the delamination interface.

Figs. 7 and 8 show that the buckling mode shapes obtained using the proposed free and constrained mode models for the delaminated VAT plates $[90\pm(0,75)]_{4s}$ and $[\pm 90]_{4s}$, respectively. Herein, the delamination position h_1/h and the delamination size c^2/ab are set to be 0.25 and 0.36, respectively. The boundary conditions and loading cases are the same as the case study presented in Table 7. The upper bounds of the residual buckling load are also predicted by the ‘*totally constrained mode*’ model [14], and are presented in Figs. 7(b) and 8(b). The buckling loads and mode shapes with constrained point effects are obtained using the ‘*partially constrained mode*’ model, and presented in Figs. 7(c) and 8(c). It was found that the contact buckling loads predicted by the ‘*partially constrained mode*’ model converge with an increasing translational stiffness K_0 . The contact buckling loads obtained are much lower than the values given by ‘*totally constrained mode*’ model. This result is expected because the delamination opening mode is not considered in the latter case, even for an off-midplane delamination. However, in the former case, the delamination opening modes remain, which leads to a significant reduction in the delamination buckling load. Meanwhile, the contact buckling loads predicted by the ‘*partially constrained mode*’ model are slightly higher than the values given by the ‘*free mode*’ model. This result is mainly due to the contact point constraints at the delamination interface. The results shown in Figs. 7 and 8 indicate that the contact constraint at the delamination interface does not increase the buckling load significantly, which has also been reported by Shahwan and Waas [20] and Suemasu et al. [32]. However, a significant difference exists between the buckling mode shapes obtained using free and partially constrained mode models. Especially for the VAT layup $[90\pm(0,75)]_{4s}$, where an asymmetric bulge can be observed in the mode shapes predicted by the ‘*partially constrained mode*’ model. Furthermore, it was observed from Figs. 7(c) and 8(c) that the residual interpenetrated area within the buckling mode shapes is fairly small, which indicates that penetration has been suppressed to a large extent. The virtual spring is applied at one or several contact points rather than the contact area, inevitably leading to the emergence of residual interpenetrated areas. However, the buckled state with sufficiently small residual interpenetrated area when contact buckling occurs can be approximated as a contact state [32, 33].

5.4 Effect of varying fibre orientation angles

This section studies the mechanism of applying tow-steered laminates to improve the buckling performance of composite plates with a single delamination. The delaminated VAT plate is clamped at all four edges and is subjected to a uniform axial compression. Herein, only an embedded delamination is considered and the normalized delamination position h_1/h is taken to be 0.5. As such, this is a mid-plane delamination, which indicates that the delamination opening and contact problem are not taken into account in the buckling analysis [23]. Four different composite layups are chosen to study: $[90\pm(10,80)]_{4s}$, $[90\pm(20,90)]_{4s}$, $[0]_{16}$ and $[\pm 45]_{4s}$. Fig. 9 shows the buckling coefficients and the buckling load reduction percentages of these four delaminated composite laminates with respect to the delamination size, which is characterized by the normalized delamination area c^2/ab . As shown in Fig. 9(a), for each layup, the buckling coefficient remains unchanged at the initial stage, and then gradually decreases with an increase in delamination size (c^2/ab). The decrease in bending stiffness induced by delamination is the main reason for the reduction in buckling load, as also explained previously. Fig. 9(b) shows the buckling load reduction percentage for each delaminated composite, in which the $[0]_{16}$ layup gives higher buckling resistance against the existence of delamination than the $[\pm 45]_{4s}$ laminate. This behaviour occurs because the bend-twist coupling effect of $[\pm 45]_{4s}$ layup is more pronounced [26], and bend-twist coupling lowers the residual buckling resistance of delaminated composite plates. Further, it is clearly seen from Fig. 9(a) that the VAT layups $[90\pm(10,80)]_{4s}$ and $[90\pm(20,90)]_{4s}$ exhibit better performance for delamination buckling resistance than the $[0]_{16}$ layup. For these two types of VAT laminates, as has been shown in many previous works [1-3, 7], the majority of compressive loading is redistributed remote from the central delamination region towards the supported edges. Such benign load redistribution enables the VAT layups to reach higher buckling resistance, even if there exists delamination. However, it is found that the VAT layup $[90\pm(10,80)]_{4s}$ initially exhibits higher buckling load due to better load redistribution, but gives less buckling resistance against delamination than the VAT layup $[90\pm(20,90)]_{4s}$ (Fig. 9(b)). This result indicates that in addition to the load redistribution induced by the non-uniform extensional stiffness distribution, the buckling behaviour of the delaminated VAT composite plate is also affected by the non-uniform bending stiffness distribution. The variable angle tow fibre angle distribution given by the VAT layup $[90\pm(20,90)]_{4s}$ exhibits more favourable bending stiffness distribution over the delamination region, and thus helps to resist delamination buckling.

A parametric study is now performed on the buckling analysis of VAT plate configurations $[90\pm(T_0, T_1)]_{4s}$ with an embedded rectangular delamination. Both T_0 and T_1 increase from 0° to 90° with a step of 10° . Herein, four different delamination sizes are examined, for which the normalized delamination area c^2/ab are 0.0, 0.25, 0.49 and 0.81, in the parametric study. In

each case, the delamination buckling loads are plotted in Fig. 10 as functions of the prebuckling stiffness. Each curve in Fig. 10 represents a series of VAT plates that is generated by varying T_1 from 0° at the left-end to 90° at the right-end, with a same value of T_0 . For comparison purposes, the buckling load and prebuckling stiffness of the delaminated VAT plates are normalized with respect to those of an intact quasi-isotropic laminate, respectively. The prebuckling stiffness E_{vat} of the VAT plate is defined as [2, 3, 7],

$$E_{\text{vat}} = \frac{a}{hb^2\Delta} \int_{-b/2}^{b/2} N_{xx}^0(a/2, y) dy \quad (31)$$

The evaluation of buckling load of the intact quasi-isotropic laminate based on an equivalent bending stiffness is given by [7, 34].

From Fig. 10, it is noted that the overall curves that represent normalized delamination buckling loads of VAT plates are nearly the same in each subfigure, albeit the buckling loads are substantially reduced with the presence of the rectangular delamination. This behaviour indicates that the mechanism (load redistribution) by which the variable stiffness properties improve the buckling load of composite plates remains in effect when delamination occurs. At different normalized delamination areas c^2/ab of 0.0, 0.25, 0.49 and 0.81, VAT layups achieve 52.3%, 59.7%, 88.9% and 76.1% improvement on the maximum buckling load over the straight-fibre laminates, respectively. Further, it is found from Fig. 10 that when the normalized value of prebuckling stiffness is between 0.4 and 1.6, the VAT configurations show more additional freedom in stiffness tailoring to achieve higher delamination buckling resistance. In addition, the VAT layups that give the maximum buckling load for each case are slightly different. It thus further implies that the buckling improvement for the delaminated VAT plates not only depends on the load redistribution, but also is affected by the local distribution of variable angle tows over the delamination region. In summary, the results shown in Fig. 10 clearly demonstrate the advantages and the potentials of applying VAT laminates to improve the buckling performance of composite laminated plates with a single delamination.

6 Conclusion

An analytical model has been developed to study the buckling behaviour of VAT composite plates with a through-the-width or an embedded rectangular delamination. The superposition method given by global and local shape functions was applied to model the displacement fields of VAT composite plates. Both free and constrained mode models were constructed to simulate delamination buckling processes. It was shown that this proposed analytical model is able to accurately capture the global, mixed and local buckling response of delaminated VAT composite plates. For the case when contact between delaminated portions occurs, a constrained point approach was employed to study the contact effect in the delamination buckling analysis. Numerical results of VAT composite plates with a single delamination were

obtained with respect to various delamination sizes and positions. Compared with the previous published works and FEM simulation results, the accuracy and efficiency of this proposed method to predict the delamination buckling loads was demonstrated. It was also found that the in-plane deformation of delaminated portions within the delamination region is vitally important for the delamination buckling analysis.

The effects of delamination size and position on the buckling response of delaminated VAT composite plates were examined through various numerical case studies. Results have shown that buckling loads decrease with an increase in delamination size. An off mid-plane delamination may further reduce the buckling load due to the occurrence of delamination opening. The residual delamination buckling load was found to be slightly increased when contact buckling occurs, and the corresponding buckling mode shape was significantly altered by the potential contact at the delamination interface. The influence of varying fibre orientation angles on the residual buckling strength of VAT composite plates with an embedded rectangular delamination was then studied. It was found that the buckling strength of composite plates with a delamination can be significantly improved by particular VAT configurations. Finally, a parametric study of VAT laminates with linearly varying fibre angles was performed. The mechanism and advantages of applying the variable stiffness concept to improve the buckling performance of delaminated composite laminates were drawn from the numerical results. The postbuckling and delamination growth problems of VAT composite plates with delaminations will be studied and presented in our future works.

Acknowledgments

Zhangming Wu wish to sincerely acknowledge the financial support from China's 1000 Young Talent Programme and the Strathclyde Chancellor's Fellowship (University of Strathclyde, Scotland). Guojun Nie wish to acknowledge the financial support under the research project from National Natural Science Foundation of China (No.11072177 and 11372225). Paul Weaver would like to thank Science Foundation Ireland for funding Varicomp project under its Research Professor Scheme.

References

- [1] Coburn BH, Wu Z, Weaver PM. Buckling analysis of stiffened variable angle tow panels. *Composite Structures* 2014; 111(11): 259-70.
- [2] Gürdal Z, Tatting BF, Wu CK. Variable stiffness composite panels: Effects of stiffness variation on the in-plane and buckling response. *Composites Part A* 2008; 39(5): 911-22.
- [3] Raju G, Wu Z, Kim BC, Weaver PM. Prebuckling and buckling analysis of variable angle tow plates with general boundary conditions. *Composite Structures* 2012; 94(9): 2961-70.
- [4] Setoodeh S, Abdalla MM, IJsselmuiden ST, Gürdal Z. Design of variable-stiffness

- composite panels for maximum buckling load. *Composite Structures* 2009; 87(1): 109-17.
- [5] Wu Z, Raju G, Weaver PM. Postbuckling analysis of variable angle tow composite plates. *International Journal of Solids and Structures* 2013; 50(10): 1770-80.
- [6] Wu Z, Raju G, Weaver PM. Framework for the buckling optimization of variable angle tow composite plates. *AIAA Journal* 2015; 53(12): 3788-804.
- [7] Wu Z, Weaver PM, Raju G, Kim BC. Buckling analysis and optimisation of variable angle tow composite plates. *Thin-Walled Structures* 2012; 60(10): 163-72.
- [8] Chai H, Babcock CD, Knauss WG. One Dimensional Modeling of Failure in Laminated Plates by Delamination Buckling. *International Journal of Solids and Structures* 1981; 17(11): 1069-83.
- [9] Simites GJ, Sallam S, Yin WL. Effect of Delamination of Axially Loaded Homogeneous Laminated Plates. *AIAA Journal* 1985; 23(9): 1437-44.
- [10] Kardomateas GA, Schmueser DW. Buckling and Postbuckling of Delaminated Composites under Compressive Loads Including Transverse-Shear Effects. *AIAA Journal* 1988; 26(3): 337-43.
- [11] Kutlu Z, Chang FK. Modeling Compression Failure of Laminated Composites Containing Multiple through-the-Width Delaminations. *Journal of Composite Materials* 1992; 26(3): 350-87.
- [12] Lee J, Gürdal Z, Griffin OH. Layer-Wise Approach for the Bifurcation Problem in Laminated Composites with Delaminations. *AIAA Journal* 1993; 31(2): 331-38.
- [13] Chattopadhyay A, Gu H. New Higher-Order Plate-Theory in Modeling Delamination Buckling of Composite Laminates. *AIAA Journal* 1994; 32(8): 1709-16.
- [14] Shu D. Buckling of multiple delaminated beams. *International Journal of Solids and Structures* 1998; 35(13): 1451-65.
- [15] Bruno D, Greco F. An asymptotic analysis of delamination buckling and growth in layered plates. *International Journal of Solids and Structures* 2000; 37(43): 6239-76.
- [16] Shivakumar KN, Whitcomb JD. Buckling of a Sublaminar in a Quasi-Isotropic Composite Laminate. *Journal of Composite Materials* 1985; 19(1): 2-18.
- [17] Chai H, Babcock CD. Two-dimensional modeling of compressive failure in delaminated laminates. *Journal of Composite Materials* 1985; 19(1): 67-98.
- [18] Yin WL, Jane KC. Refined buckling and postbuckling analysis of 2-Dimensional delaminations—I. analysis and validation. *International Journal of Solids and Structures* 1992; 29(5): 591-610.
- [19] Chai H. Contact buckling and postbuckling of thin rectangular plates. *Journal of the Mechanics and Physics of Solids* 2001; 49(2): 209-30.
- [20] Shahwan KW, Waas AM. A mechanical model for the buckling of unilaterally constrained rectangular plates. *International Journal of Solids and Structures* 1994; 31(1): 75-87.

- [21] Suemasu H, Irie T, Ishikawa T. Buckling and Post-buckling Behavior of Composite Plates Containing Multiple Delaminations. *Journal of Composite Materials* 2009; 43(2): 191-202.
- [22] Suemasu H, Kumagai T. Compressive behavior of multiply delaminated composite laminates part 2: Finite element analysis. *AIAA Journal* 1998; 36(7): 1286-90.
- [23] Suemasu H, Kumagai T, Gozu K. Compressive behavior of multiply delaminated composite laminates part 1: Experiment and analytical development. *AIAA Journal* 1998; 36(7): 1279-85.
- [24] Kim H, Kedward KT. A method for modeling the local and global buckling of delaminated composite plates. *Composite Structures* 1999; 44(1): 43-53.
- [25] Kharazi M, Ovesy HR, Taghizadeh M. Buckling of the composite laminates containing through-the-width delaminations using different plate theories. *Composite Structures* 2010; 92(5): 1176-83.
- [26] Ovesy HR, Kharazi M, Taghizadeh M. Semi-analytical Buckling Analysis of Clamped Composite Plates Containing Embedded Rectangular and Circular Delaminations. *Mechanics of Advanced Materials and Structures* 2010; 17(5): 343-52.
- [27] Butler R, Baker N, Liu W. Damage Tolerance of Buckling Optimized Variable Angle Tow Panels. In: 50th AIAA/ASME/ASCE/AHS/ASC Structures, Structural Dynamics, and Materials Conference; 2009. p. 1-10.
- [28] Yazdani S, Rust WJH, Wriggers P. Delamination growth in composite laminates of variable stiffness. *International Journal for Numerical Methods in Engineering* 2016; 108(11): 1406-24.
- [29] Gürdal Z, Olmedo R. In-plane response of laminates with spatially varying fiber orientations: Variable stiffness concept. *AIAA Journal* 1993; 31(4): 751-8.
- [30] Reddy JN. *Mechanics of laminated composite plates and shells theory and analysis*. 2nd ed. New York: CRC press; 2004.
- [31] Ashton JE. Approximate solutions for unsymmetrically laminated plates. *Journal of Composite Materials* 1969; 3(1): 189-91.
- [32] Suemasu H, Gozu K, Hayashi K, Ishikawa T. Compressive buckling of rectangular composite plates with a free-edge delamination. *AIAA Journal* 1995; 33(2): 312-19.
- [33] Suemasu H. Postbuckling behaviors of composite panels with multiple delaminations. *Journal of Composite Materials* 1993; 27 (11): 1077-96.
- [34] Diaconu CG, Weaver PM. Approximate solution and optimum design of compression-loaded, postbuckled laminated composite plates. *AIAA Journal* 2005; 43(4): 906-14.

Figure caption

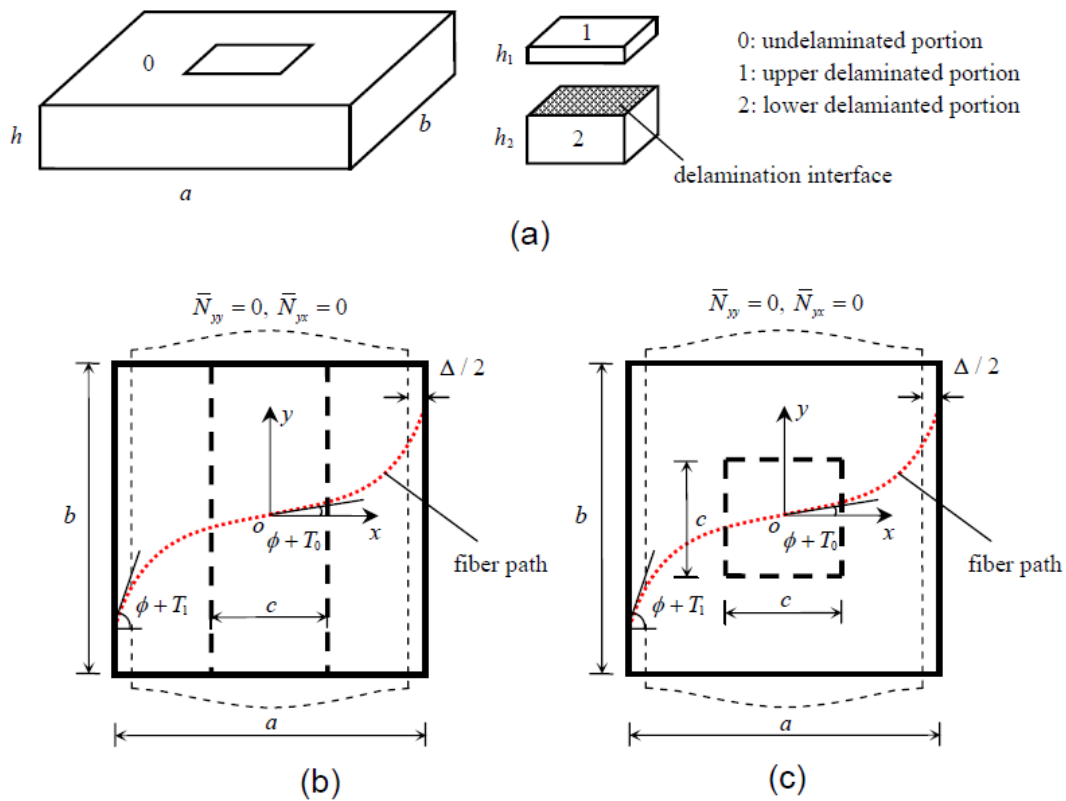


Fig.1 The geometry and in-plane boundary conditions of a VAT composite plate with a single delamination: (a) Division of the delaminated VAT plate into three portions; (b) VAT plate with a through-the-width delamination; (c) VAT plate with an embedded rectangular delamination.

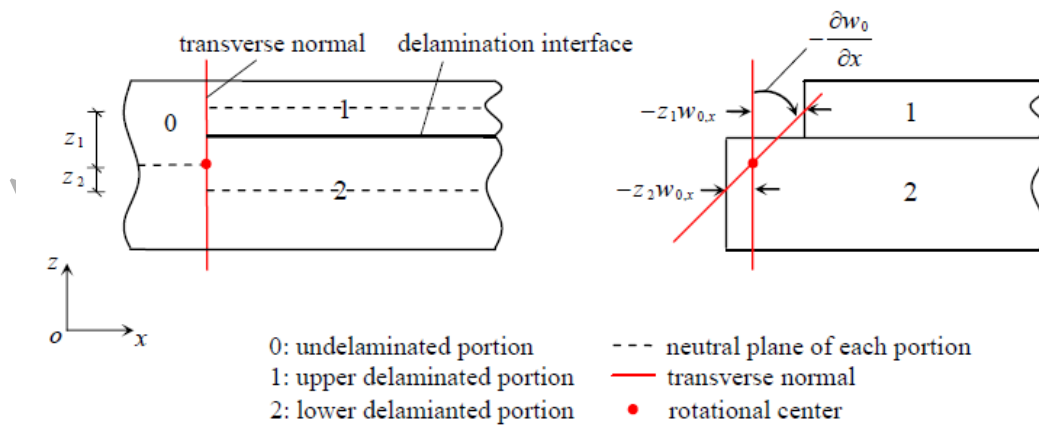


Fig. 2 In-plane deformation of delaminated portion on the delamination edge.

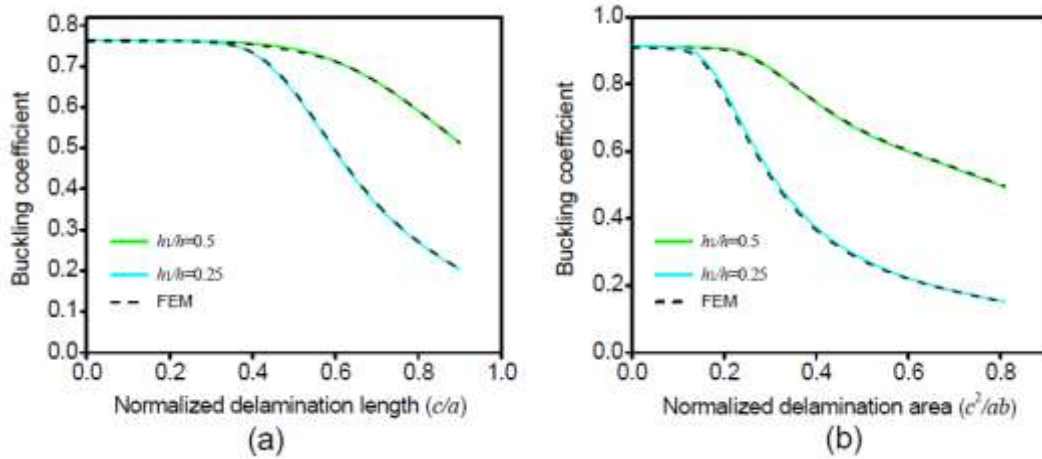


Fig. 3 The buckling coefficients of two VAT plates vary with respect to normalized delamination size or area (c/b or c^2/ab) for two different delamination positions ($h_1/h=0.5$ or 0.25): (a) VAT plate $[\pm(0,30)]_{4s}$ with a through-the-width delamination; (b) VAT plate $[\pm(0,90)]_{4s}$ with an embedded rectangular delamination.

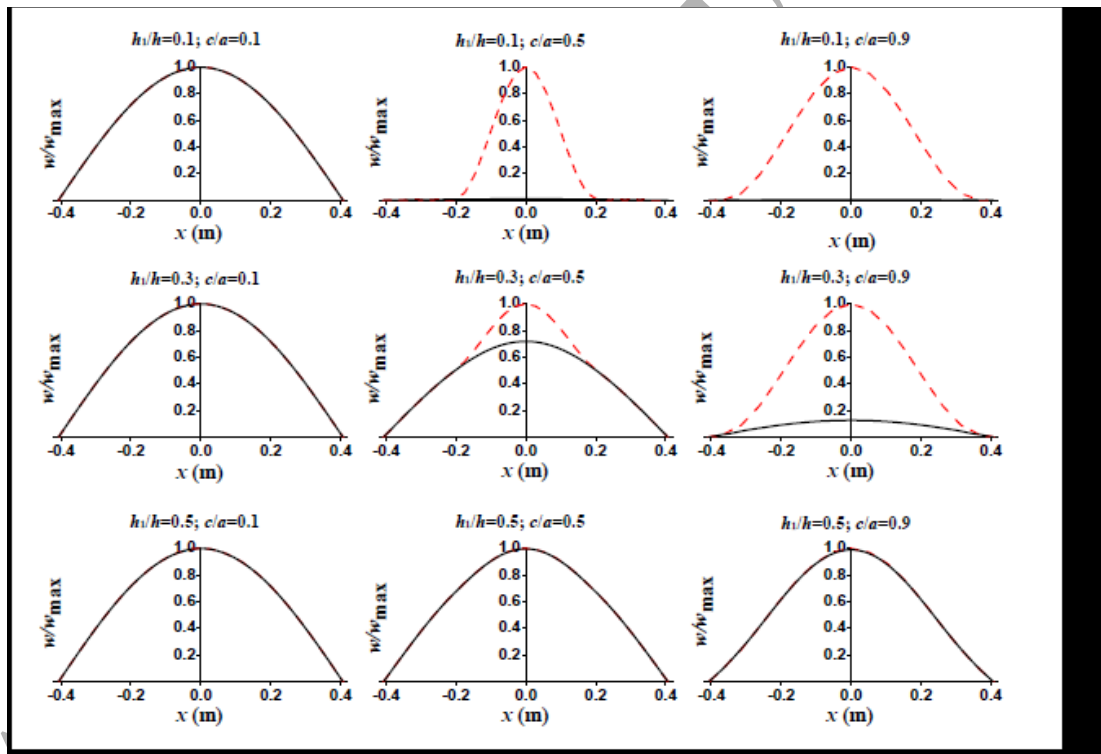


Fig. 4 The cross-sections of the buckling mode shapes along the x -axis direction ($y=0.0$) obtained by the present method for the delaminated composite plate $[0]_{20}$ with different combinations of normalized delamination position/length. The red dash curve denotes results of buckling mode shapes of the upper sublaminate.

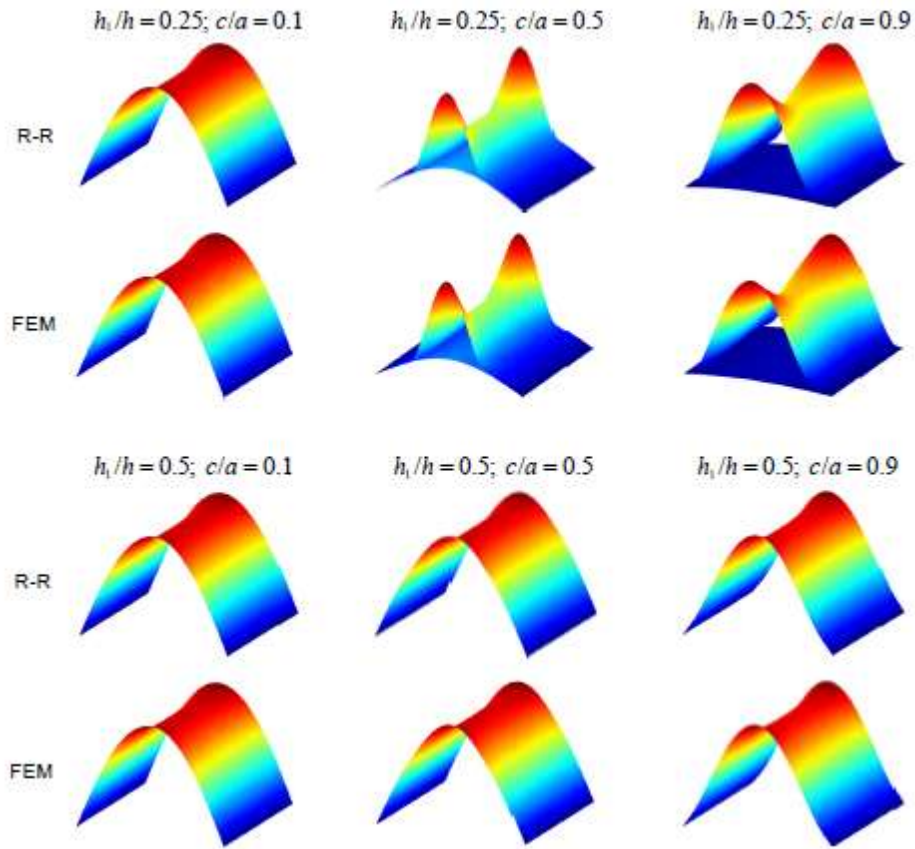


Fig. 5 Comparison of buckling mode shapes of a simply supported VAT beam-plates $[\pm(0,30)]_{4s}$ with a through-the-width delamination obtained using present analytical model and FEM for different combinations of normalized delamination position/length

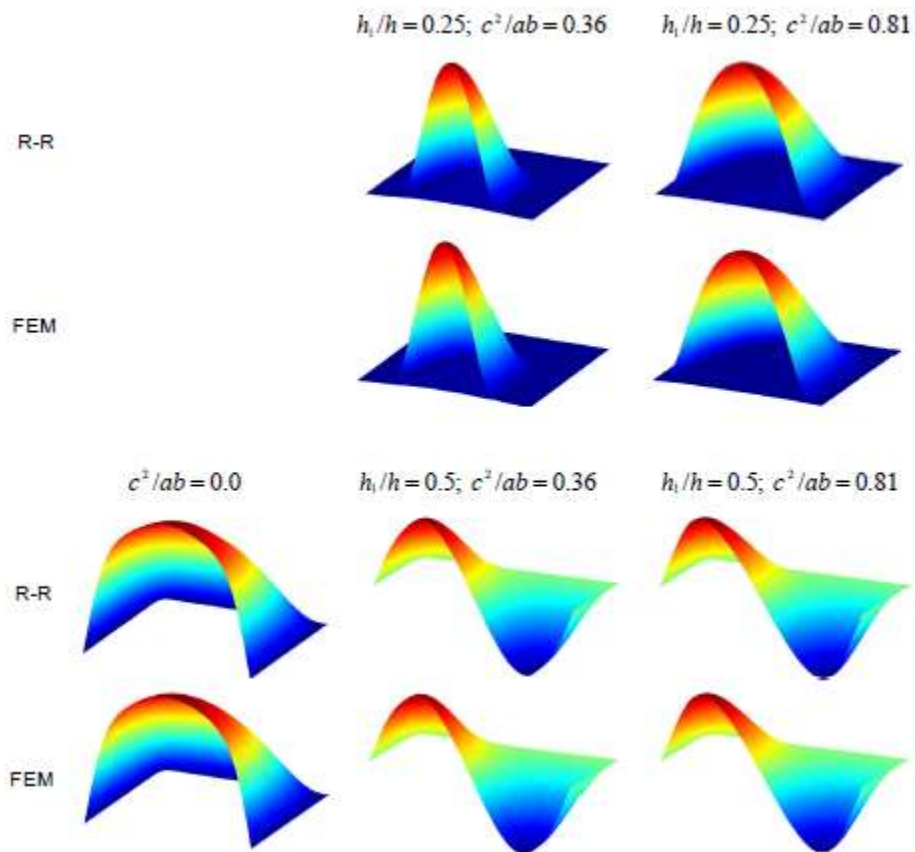


Fig. 6 Comparison of buckling mode shapes of a simply supported VAT plates $[\pm(0,90)]_{4s}$ with an embedded delamination obtained using the proposed model and FEM for different combinations of normalized delamination position/area.

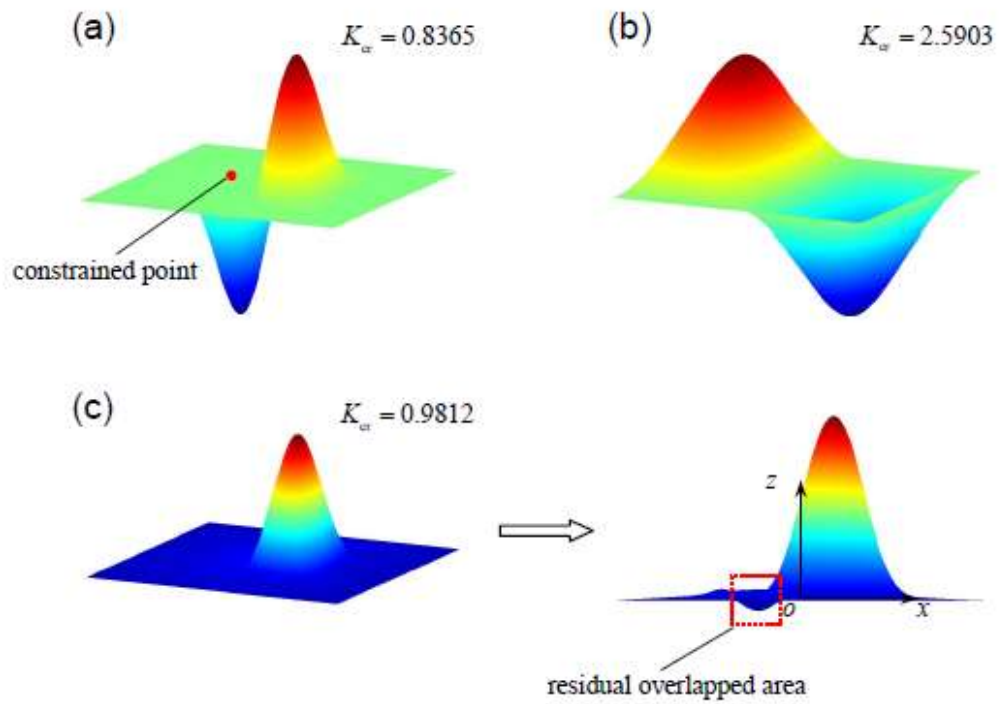


Fig. 7 Buckling mode shapes obtained using free and constrained mode models for a VAT layup $[90\pm(0,75)]_{4s}$: (a) free mode model; (b) totally constrained mode model; (c) partially constrained mode model

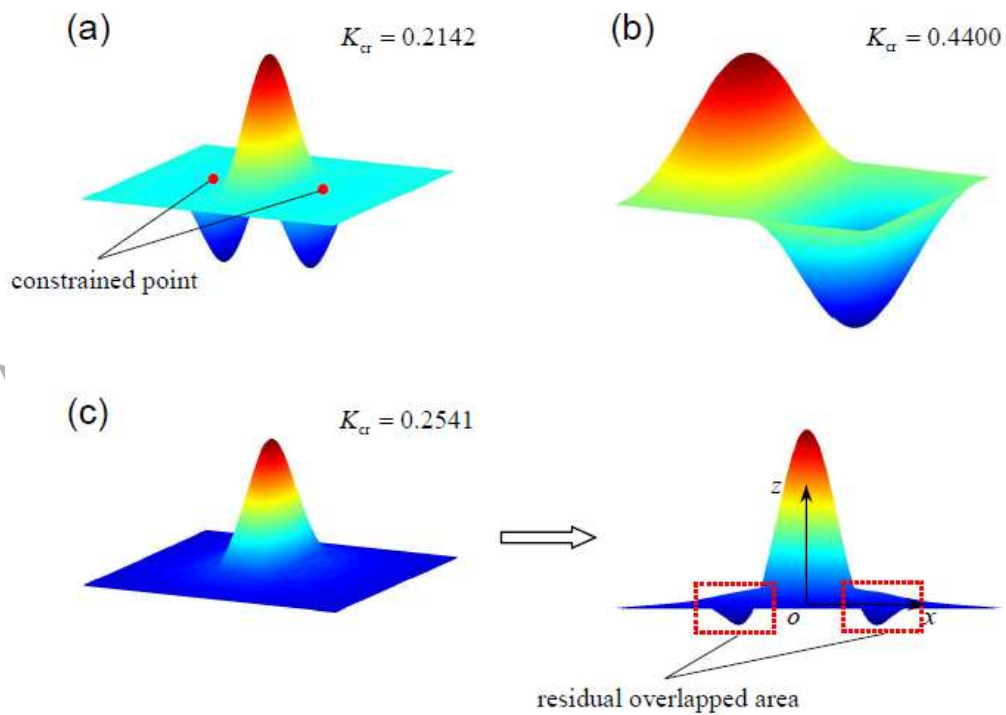


Fig. 8 Buckling mode shapes obtained using free and constrained mode models for a VAT layup $[\pm 90]_{4s}$: (a) free mode model; (b) totally constrained mode model; (c) partially constrained mode model

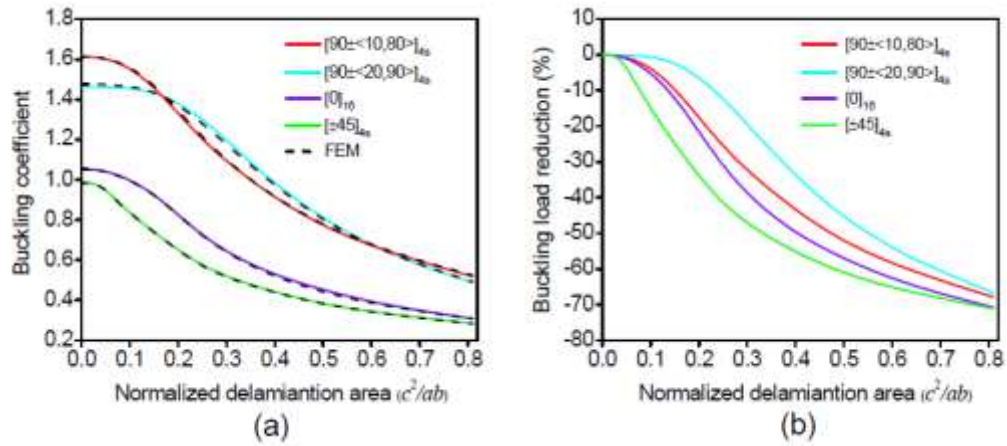


Fig. 9 Variations in buckling coefficient and buckling load reduction with the normalized delamination area (c^2/ab) for different layup configurations: (a) buckling coefficient versus normalized delamination area; (b) buckling load reduction versus normalized delamination area

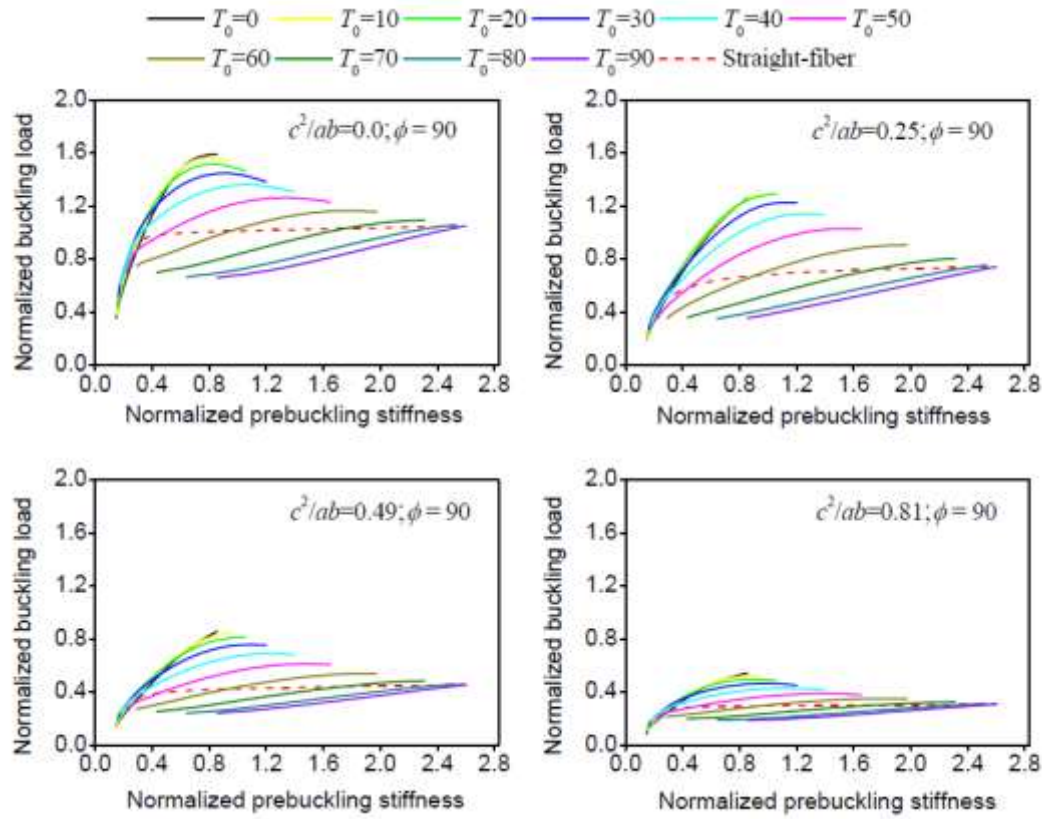


Fig. 10 Normalized buckling load versus normalized prebuckling stiffness of all the VAT configurations $[90 \pm \langle T_0, T_1 \rangle]_{4s}$ with a midplane embedded delamination at different values of normalized delamination area (c^2/ab).

Table

Table 1 The normalized critical buckling load of a two edges clamped and two edges free (CFCF) composite plate $[0]_{20}$ obtained using different number of terms for the global and local shape functions

$M(\bar{N})=3$	$M(\bar{N})=5$	$M(\bar{N})=7$	$M(\bar{N})=9$	Simiteses et al.[9]	Lee et al. [12]	FEM
$\bar{M}(\bar{N})=3$	$\bar{M}(\bar{N})=5$	$\bar{M}(\bar{N})=7$	$\bar{M}(\bar{N})=9$			
0.5422	0.5412	0.5409	0.5408	0.5411	0.5413	0.5412

Table 2 The normalized critical buckling loads of a two edges simply-supported and two edges free (SFSF) composite plates $[0]_{20}$ with a through-the-width delamination

h_1/h	c/a	Present solution	FEM	Simiteses et al.[9]	Shu [14]
0.4	0.0	1.0000	1.0000	1.0000	1.0000
	0.2	0.9996	0.9993	0.9997	0.9997

0.4	0.9901	0.9895	0.9902	0.9902
0.6	0.9196	0.9161	0.9198	0.9198
0.8	0.7263	0.7238	0.7264	0.7264

Table 3 The normalized critical buckling loads of a composite beam-plates $[0]_{20}$ with a through-the-width delamination under different boundary conditions

B.C.	h_1/h	c/a	0.0	0.1	0.2	0.3	0.4	0.5	0.6	0.7	0.8	0.9
SF	0.1	Simitses et al.[9]	1.0000	1.0000	0.9723	0.4432	0.2494	0.1596	0.1109	0.0815	0.0624	0.0493
		R-R	1.0000	0.9999	0.9728	0.4434	0.2496	0.1597	0.1109	0.0815	0.0624	0.0493
	0.3	Simitses et al.[9]	1.0000	1.0000	0.9997	0.9971	0.9827	0.9402	0.8149	0.6486	0.5118	0.4106
		R-R	1.0000	0.9999	0.9996	0.9969	0.9850	0.9401	0.8151	0.6487	0.5120	0.4108
	0.5	Simitses et al.[9]	1.0000	0.9999	0.9997	0.9980	0.9912	0.9729	0.9343	0.8703	0.7867	0.6966
		R-R	1.0000	0.9999	0.9997	0.9979	0.9912	0.9726	0.9345	0.8706	0.7870	0.6970
CF	0.1	Simitses et al.[9]	1.0000	0.9799	0.2495	0.1109	0.0624	0.0400	0.0278	0.0204	0.0156	0.0123
		R-R	1.0000	0.9801	0.2493	0.1109	0.0624	0.0399	0.0278	0.0204	0.0156	0.0123
	0.3	Simitses et al.[9]	1.0000	0.9998	0.9924	0.8582	0.5314	0.3469	0.2435	0.1804	0.1390	0.1105
		R-R	1.0000	0.9996	0.9922	0.8587	0.5315	0.3469	0.2435	0.1804	0.1390	0.1105
	0.5	Simitses et al.[9]	1.0000	0.9999	0.9956	0.9638	0.8481	0.6896	0.5411	0.4310	0.3514	0.2923
		R-R	1.0000	0.9998	0.9955	0.9639	0.8484	0.6897	0.5412	0.4309	0.3522	0.2934

Table 4 The normalized critical buckling loads of an angle-ply composite plate $[\pm 45]_{4s}$ with a through-the-width delamination for different combinations of normalized delamination position/length.

h_1/h	c/a	0.0	0.1	0.2	0.3	0.4	0.5	0.6	0.7	0.8	0.9
0.25	R-R (without in-plane motion)	1.0000	0.8849	0.7493	0.6350	0.5500	0.5057	0.4579	0.4006	0.3322	0.2702

	R-R (with in-plane motion)	1.0000	0.9995	0.9978	0.9906	0.9562	0.8741	0.6710	0.4969	0.3764	0.2927
	FEM	1.0000	0.9992	0.9981	0.9900	0.9577	0.8716	0.6699	0.4861	0.3732	0.2930
	R-R (without in-plane motion)	1.0000	0.8364	0.6260	0.4564	0.3638	0.3175	0.2916	0.2760	0.2648	0.2598
0.5	R-R (with in-plane motion)	1.0000	0.9994	0.9974	0.9896	0.9712	0.9383	0.8876	0.8188	0.7375	0.6551
	FEM	1.0000	0.9986	0.9970	0.9884	0.9748	0.9318	0.8839	0.8107	0.7332	0.6534

Table 5 The normalized critical buckling loads of a VAT composite plate $[\pm(0,30)]_{4s}$ with a through-the-width delamination for different combinations of normalized delamination position/length.

h_1/h	c/a	0.0	0.1	0.2	0.3	0.4	0.5	0.6	0.7	0.8	0.9
	R-R (without in-plane motion)	1.0000	0.8871	0.7582	0.6402	0.5525	0.4918	0.4415	0.3819	0.3115	0.2476
0.25	R-R (with in-plane motion)	1.0000	0.9999	0.9997	0.9968	0.9794	0.8441	0.6355	0.4636	0.3469	0.2654
	FEM	1.0000	0.9999	0.9991	0.9954	0.9801	0.8516	0.6423	0.4676	0.3493	0.2668
	R-R (without in-plane motion)	1.0000	0.8428	0.6536	0.4835	0.3708	0.2982	0.2784	0.2625	0.2546	0.2512
0.5	R-R (with in-plane motion)	1.0000	1.0000	0.9999	0.9983	0.9924	0.9764	0.9384	0.8705	0.7763	0.6711
	FEM	1.0000	0.9999	0.9999	0.9987	0.9893	0.9675	0.9389	0.8714	0.7771	0.6715

Table 6 The normalized critical buckling loads of an angle-ply composite plate $[\pm 45]_{4s}$ with an embedded rectangular delamination for different combinations of normalized delamination position/area.

h_1/h	c^2/ab	0.0	0.01	0.04	0.09	0.16	0.25	0.36	0.49	0.64	0.81
	R-R	1.0000	0.9999	0.9993	0.9785	0.5782	0.3701	0.2573	0.1894	0.1453	0.1151
0.25	FEM	1.0000	1.0000	0.9992	0.9595	0.5640	0.3673	0.2551	0.1890	0.1440	0.1147
	R-R	1.0000	0.9999	0.9993	0.9974	0.9906	0.8983	0.7112	0.6335	0.5486	0.4674
0.5	FEM	1.0000	0.9999	0.9995	0.9977	0.9857	0.8923	0.7146	0.6385	0.5428	0.4629

Table 7 The normalized critical buckling loads of a VAT composite plate $[\pm(0,90)]_{4s}$ with an embedded rectangular delamination for different combinations of normalized delamination position/area.

h_1/h	c^2/ab	0.0	0.01	0.04	0.09	0.16	0.25	0.36	0.49	0.64	0.81
	R-R	1.0000	0.9989	0.9978	0.9936	0.9909	0.6993	0.4444	0.3017	0.2180	0.1659
0.25	FEM	1.0000	0.9991	0.9981	0.9963	0.9821	0.6859	0.4360	0.2972	0.2180	0.1655
	R-R	1.0000	1.0000	0.9997	0.9975	0.9950	0.9915	0.8580	0.7150	0.6337	0.5392
0.5	FEM	1.0000	0.9999	0.9999	0.9997	0.9983	0.9883	0.8635	0.7229	0.6398	0.5453